An evaluation of liquid cloud droplet effective radius derived from MODIS, airborne remote sensing and in situ measurements from CAMP²Ex

Dongwei Fu[1], Larry Di Girolamo[1], Robert M. Rauber[1], Greg M. McFarquhar[2,3], Stephen W. Nesbitt[1], Jesse Loveridge[1], Yulan Hong[1], Bastiaan van Diedenhoven[4], Brian Cairns[5], Mikhail D. Alexandrov[5], Paul Lawson[6], Sarah Woods[6], Simone Tanelli[7], Sebastian Schmidt[8,9], Chris Hostetler[10], Amy Jo Scarino[11]

[1]Department of Atmospheric Sciences, University of Illinois Urbana-Champaign, Urbana, Illinois, USA.
[2]Cooperative Institute for Severe and High Impact Weather Research and Operations, The University of Oklahoma, Norman, Oklahoma, USA.
[3]School of Meteorology, The University of Oklahoma, Norman, Oklahoma, USA.
[4]SRON Netherlands Institute for Space Research, Leiden, The Netherlands.
[5]NASA Goddard Institute for Space Studies, New York City, New York, USA.
[6]Stratton Park Engineering Company, Inc., Boulder, Colorado, USA.
[7]Jet Propulsion Laboratory, Pasadena, California, USA.
[8]Department of Atmospheric and Oceanic Sciences, University of Colorado Boulder, Boulder, Colorado, USA.
[9]Laboratory for Atmospheric and Space Physics, University of Colorado Boulder, Boulder, Colorado, USA.
[10]NASA Langley Research Center, Hampton, Virginia, USA.
[11]Science Systems and Applications, Inc, Hampton, Virginia. USA.

Correspondence to: Dongwei Fu (dfu3@illinois.edu)

Abstract. The cloud drop effective radius, Re, of the drop size distribution derived from passive satellite sensors is a key variable used in climate research. Validation of these satellite products often took place in stratiform cloud conditions that favored the assumption of cloud horizontal homogeneity used by the retrieval techniques. However, many studies point to concerns of significant biases in retrieved Re arising from cloud heterogeneity, for example, in cumulus cloud fields. Here, we examine data collected during the 2019 Cloud, Aerosol and Monsoon Processes Philippines Experiment (CAMP²Ex), which, in part, targeted the objective of providing the first detailed evaluation of Re retrieved across multiple platforms and techniques in a cumulus and congestus cloud region. Our evaluation consists of cross comparisons of Re between the MODerate resolution Imaging Spectroradiometer (MODIS) onboard the Terra satellite, the Research Scanning Polarimeter (RSP) onboard the NASA P-3 aircraft, and in situ measurements from both the P-3 and Learjet aircrafts that are all taken in close space-time proximity of the same cloud fields. A particular advantage of our approach lies in RSP's capability to retrieve Re using a bi-spectral MODIS approach and a polarimetric approach, which allows for evaluating bi-spectral and polarimetric Re retrievals from an airborne perspective using the same samples.

Averaged over all P-3 flight segments examined here for warm clouds, the RSP-polarimetric, in situ, and the bias-adjusted MODIS method of Fu et al. (2019) show comparable median (mean and standard deviations) of Re samples of 9.6 (10.2 ± 4.0) μm, 11.0 (13.6 ± 11.3) μm, and 10.4 (10.8 ± 3.8) μm, respectively. These values are far lower than 15.1 (16.2 ± 5.5) μm and 17.2 (17.7 ± 5.7) μm from the bi-spectral retrievals of RSP and MODIS, respectively. Similar results are observed when Re is segregated by cloud top height and in detailed case studies. The clouds sampled during CAMP²Ex consist of mostly small (mean transect length ~1.4 km) and low clouds (mean cloud top height ~ 1 km),

40   which had more numerous small clouds than the trade wind cumuli sampled in past field campaigns such as Rain in Shallow Cumulus over the Ocean (RICO) and the Indian Ocean Experiment (INDOEX). The overestimates of *Re* from RSP bi-spectral technique compared to polarimetric technique increased as cloud size and cloud optical depth decreased. Drizzle, cloud top bumpiness and solar-zenith angle, however, are not closely correlated with the overestimate of bi-spectral *Re*. We show that for shallow clouds that dominate the liquid cloud cover for the CAMP^{2}Ex

45   region and period, 3-D radiative ~~pathways~~transfer and cloud heterogeneity, particularly for the optically thin and small clouds, appear to be the leading cause for the large positive biases in bi-spectral retrievals. Because this bias varies with the underlying structure of the cloud field, caution continues to be warranted in studies that use bi-spectral *Re* retrievals in cumulus cloud fields.

1 Introduction

50   Satellite retrieved cloud properties have been critical in advancing the understanding of the role of clouds in the Earth's climate system. Still, the role of clouds in a changing climate remains a dominant source of uncertainty in climate change predictions (IPCC, 2013). Efforts to improve the accuracy of our satellite record of cloud properties continue to be called for (Ohring et al. 2005; NASEM 2018). This includes the record of cloud droplet effective radius (*Re*) of the drop size distribution. Satellite retrieved *Re*, owing to its wide spatial coverage and continuous monitoring

55   record, has been applied for a wide range of studies such as estimating aerosol-cloud interactions (e.g., Menon et al. 2008; Ross et al. 2018; IPCC 2013) and evaluating model parameterizations (e.g., Ban-Weiss et al. 2014, Suzuki et al. 2013). By far the dominant approach for retrieving *Re* from space has been based on the bi-spectral technique of Nakajima and King (1990), which simultaneously retrieves cloud optical thickness (COT) and *Re* from visible/near infrared (VNIR) and shortwave infrared (SWIR) radiances. It has been applied to sensors such as the Advanced Very

60   High-Resolution Radiometer (AVHRR, Rossow and Schiffer 1991), the Moderate Resolution Imaging Spectroradiometer (MODIS, Platnick et al. 2003), and newer sensors such as the Visible Infrared Imaging Radiometer Suite (VIIRS, Cao et al. 2014) and the Advanced Himawari Imager (AHI, Bessho et al. 2016). Therefore, the longest records (spanning nearly four decades) of observations for cloud optical and microphysical properties are derived from the bi-spectral technique. Given its legacy and likely continued use in the future, it is essential to assess the error

65   characteristics of the bi-spectral approach to advance the understanding of climate science, particularly as it applies to cloud feedbacks (e.g., Tan et al. 2019) and aerosol-cloud interactions (e.g., Menon et al. 2008; Gryspeerdt et al. 2019).

    There have been numerous studies aimed at understanding the error characteristics of *Re* retrieved from the bi-spectral technique. The largest errors are expected to occur whenever nature substantially deviates from the

70   assumptions used by the bi-spectral technique, such as horizontally homogeneous clouds (i.e., 1-D radiative transfer is used as the forward model in this retrieval algorithm), vertically homogeneous clouds, and a single-mode drop size distribution. Evaluations of *Re* from past field campaigns (e.g., Nakajima et al. 1991; Platnick and Valero 1995; Painemal and Zuidema 2011; McBride et al. 2012, Witte et al. 2018) show a ~ - 0.2 – 3 μm (~ - 2% - 40%) bias for MODIS and MODIS-like instruments, mostly for marine stratiform clouds under high sun conditions – conditions that

75   are most favorable for the 1-D assumption (e.g., Loeb et al. 1998; Di Girolamo et al. 2010). 3-D radiative transfer

simulations suggest larger biases in the cumulus cloud fields that can reach ~100% (e.g., Marshak et al. 2006), with the bias closely related to cloud heterogeneity and solar zenith angles. Under low sun conditions, Ahn et al. (2018) recently compared MODIS *Re* with airborne in-situ measurements over the Southern Ocean and reported a bias of 8 to 13 μm for non-drizzling clouds. A global perspective of the bias in MODIS *Re* was provided by Liang et al. (2015), who estimated zonal mean biases ranging from 2 to 11 μm by fusing data from MODIS and the Multi-angle Imaging SpectroRadiometer (MISR, Diner et al. 1998). Their approach was further extended to regional estimates of the bias across the globe by Fu et al. (2019), which showed dependence of the *Re* bias on the cloud regime (i.e., larger bias in more cumuliform regimes). Fu et al. (2019) showed that the largest *Re* biases (up to +10 μm) occur over the tropical western pacific, which curiously is also the region where MODIS pixels detected as cloudy have the largest failures rates (up to 40%) in retrieving cloud optical and microphysical properties (Cho et al. 2015). Since liquid water clouds in this region are dominated by cumulus and cumulus congestus clouds, a field campaign that in part targets the evaluation of *Re* retrievals for these clouds was warranted.

The Cloud, Aerosol and Monsoon Processes Philippines Experiment (CAMP²Ex; Di Girolamo et al. 2015), which took place in the Philippines and its surrounding waters from August to October of 2019, offers an opportunity for evaluating and understanding satellite derived cloud optical and microphysical properties in a heterogeneous environment. Remote sensing and in-situ measurements of the clouds and aerosol fields were retrieved by the NASA P-3 and Learjet aircraft platforms. In this study, we focus on evaluating remotely sensed *Re* retrievals for warm cumulus and congestus clouds sampled during CAMP²Ex. Over the past several decades, satellite retrievals have not been evaluated in cumulus cloud fields, largely because of the difficulties in doing so. The fast-changing nature and complex cloud top structures of these clouds posed challenges for good cloud-top coordination between satellite observations and airborne/in-situ measurements. CAMP²Ex provided tight coordination between Terra overpasses and the P-3 aircraft that carried the Research Scanning Polarimeter (RSP, Cairns et al. 1999). RSP provides bi-spectral and polarimetric retrievals of *Re*. The polarimetric *Re* is retrieved from multi-angle polarized radiances that are sensitive to single scattering. Past studies have indicated that the accuracy of polarimetric retrievals is less affected by the assumptions of plane parallel and homogeneous clouds than the bi-spectral technique (Bréon and Doutriaux-Boucher, 2005; Alexandrov et al. 2012, Alexandrov et al. 2015). In this study, we rely on the RSP polarimetric *Re* to assess the RSP bi-spectral *Re* and MODIS *Re*. In addition, in situ derived *Re* from the P-3 and the Learjet platforms can also help to assess the performance of both the RSP retrieved *Re* and MODIS retrieved *Re*. There are several merits in cross-evaluating remotely sensed *Re* through comparison of data from different techniques and platforms: 1) RSP alone allows us to assess the performance of the bi-spectral technique against the polarimetric technique without concerns on spatial and temporal collocation mismatches; 2) Comparing the MODIS bi-spectral *Re* against RSP bi-spectral *Re* can further assess the impact of measurement resolution (i.e., satellite vs. airborne) on the retrievals; and 3) P-3 in situ derived *Re* can assess the performance of the RSP polarimetric *Re* from the same airborne platform, whereas the Learjet in situ derived *Re* can further supplement the in situ derived *Re* from a different airborne platform. Along with RSP, the P-3 carried the High Spectral Resolution Lidar 2 (HSRL-2, Hair et al. 2008, Burton et al. 2018), which provided measurements of aerosol properties and cloud top heights, and the Airborne Third Generation Precipitation Radar (APR-3, Durden et al. 2020), which provided precipitation information. Together they

help to further investigate underlying relationships between the *Re* differences (difference between RSP bi-spectral and polarimetric *Re*) and potential impact factors such as 3-D effects and drizzle. Thus, the objective of this study is to better understand the error characteristics of satellite retrieved *Re* and provide insights on future satellite instrumental designs by comparing bi-spectrally retrieved satellite *Re* with that from aircraft remote sensing and in situ measurements. In doing so, this study addresses the following questions:

1) What are the microphysical and macrophyscial properties of warm cumulus and congestus clouds sampled from a variety of observing systems during CAMP²Ex?

2) What are the relative errors between *Re* values retrieved from the bi-spectral techniques of MODIS and RSP, the bias-corrected MODIS *Re* technique of Fu et al. (2019), the RSP polarimetric technique, and in situ cloud probes?

3) How do these relative errors depend on factors such as cloud horizontal and vertical heterogeneity and drizzle?

This paper is structured as follow~~sed~~: In Sect. 2, the dataset and the methodology used in this analysis are~~is~~ presented. In Sect. 3, we first provide an overview of the sampled clouds~~'s~~ characteristics, and then examine the detailed behaviors of individual cloud fields, while focusing on the differences of the retrieved *Re* from different techniques. In Sect. 4, we further examine the dependence of the observed *Re* differences between the RSP polarimetric *Re* and bi-spectral *Re* on various impact factors (e.g., 3-D effects, sub-pixel heterogeneity, drizzle, etc.), and discuss the consistency of representativeness of the *Re* retrieved from different techniques during CAMP²Ex. Finally, conclusions ~~is~~ are provided in Sect. 5.

2 Data and methodology

2.1 CAMP²Ex dataset

~~The~~ CAMP²Ex ~~region~~ was focused on the Philippines and its nearby waters, from approximately 6° N to 23° N, and 116° E to 128.5° E. 19 research flights of the NASA P-3 and 13 flights of the SPEC Learjet were flown during CAMP²Ex, 12 of which were joint missions. Sampled cloud fields include tropical storm convective cores, cold pools, broken shallow cumulus and congestus clouds. Frequent cirrus and altostratus clouds were also present during the flights. The P-3 platform was equipped with an array of instruments that included remote sensing instruments such as the RSP, HSRL-2, APR-3, and the SPN-S spectral pyranometer (Badosa et al., 2014; Norgren et al. 2022). In situ probes such as the Fast Cloud Droplet Probe (FCDP, O'Connor et al. 2008) and 2-D Stereo Probes (2D-S, Lawson et al. 2006) were also installed on the P-3. The SPEC Learjet carried similar cloud microphysical probes as the P-3. There were 14 research flights (RF; Fig. 1) ~~for~~ of the P-3 that were coordinated with Terra-MODIS overpass~~es~~. Terra MODIS was chosen for the analysis rather than the Aqua MODIS or VIIRS because the overpass time of the latter two sensors occurs in the afternoon when cirrus is more frequent and when the aircraft was returning to base; therefore, the sampling was not favorable. In addition, we applied the bias-adjustment technique of Fu et al. (2019), which was specifically developed for the Terra MODIS *Re*.
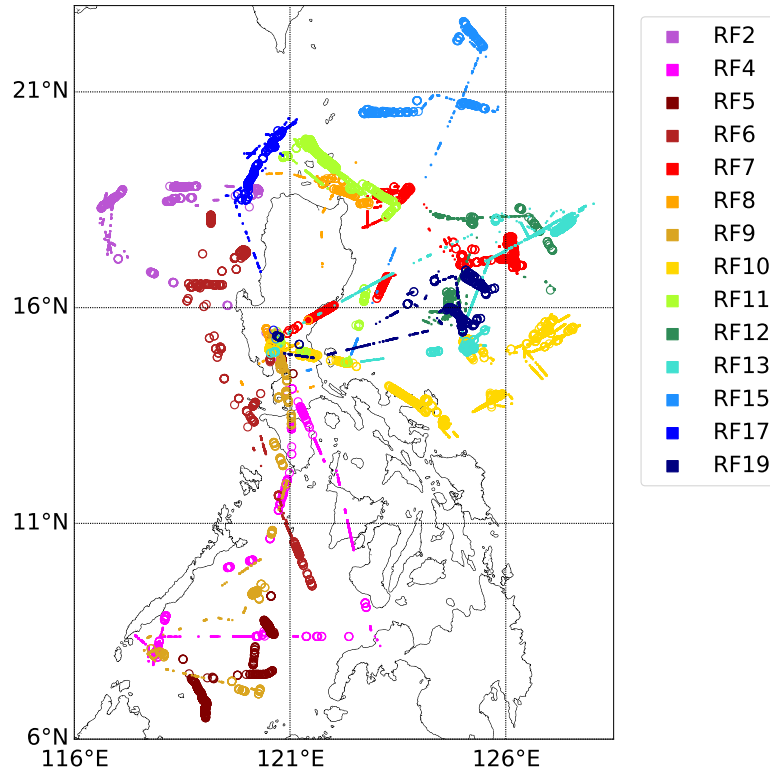
Figure 1. Flight tracks for 14 P-3 research flights with the Terra-MODIS overpass coordination over the CAMP^{2}Ex region. Dots indicate remote sensing legs with valid RSP retrievals; hollow circles indicate in situ legs with FCDP number concentration > 10 /cm^3.

Table 1. CAMP^{2}Ex P-3 research flights with successful coordination between P-3 and MODIS. RFs in bold indicates successful overlap between RSP sampling and MODIS.

Flight Date (by UTC start)	No.	Geographic Regions
2019-08-27	**2**	NE South China Sea, W Luzon
2019-08-30	**4**	W, E Sulu Sea
2019-09-04	5	S Sulu Sea
2019-09-06	6	W Luzon, Mindoro Strait
2019-09-08	**7**	NE Luzon, far E of Luzon
2019-09-13	**8**	N,S Luzon, Lingayen Gulf
2019-09-15	**9**	W,S Sulu Sea
2019-09-16	**10**	Mt Mayon then NE into Philippine Sea
2019-09-19	**11**	N Luzon, transit along E Luzon
2019-09-21	**12**	Far E of Luzon
2019-09-23	**13**	Far E of Luzon, then S toward SE Luzon region
2019-09-27	**15**	Far NE of Luzon
2019-10-01	**17**	NW, N Luzon
2019-10-05	**19**	Far E of Luzon

2.1.1 RSP cloud retrievals

RSP (Cairns et al. 1999) is a multi-angle multi-spectral polarimeter that provides along-track scans at up to 152 views between view zenith angles of about $\pm 60°$. It measures total and polarized reflectance at nine visible and shortwave infrared channels. RSP retrieves both polarimetric and bi-spectral Re. The RSP retrieves polarimetric Re using polarized reflectance of the cloud bow with scattering angles ranging between 137 and 165 degrees. The shape of the cloud bow is dominated by the single scattering properties of cloud particles, which ~~are~~is less susceptible to uncertainties caused by 3-D radiative effects and aerosol loading (Alexandrov et al. 2012). The polarimetric technique uses a pre-calculated look-up table of single-scattering polarized phase functions with various Re, Ve (effective variance) and scattering angles. Polarimetric Re is retrieved by applying a parametric fitting to determine the relation between the phase function and the observed polarized reflectance. For the bi-spectral technique, like MODIS, the RSP uses the nadir reflectance at 865 nm (channel with negligible absorption by water) and at 1588 nm and 2260 nm (channels with strong absorption by water) to retrieve Re and COT from a look-up table of pre-calculated reflectance of the two channels as a function of Re, COT and sun-view geometry. In this analysis we mostly focus on the bi-spectral Re retrievals from ~~the~~ 2260 nm. Note the maximum Re for both polarimetric and bi-spectral look-up tables is 30 μm. For COT, the standard COT product from RSP is retrieved using total reflectances and polarimetric Re; RSP also reports the bi-spectral retrieved COT. The RSP retrievals are reported at ~0.8 second intervals (~1.2 Hz), which depending on aircraft platform altitude and air speed, result~~sing~~ in spatial resolutions of ~120 meters during CAMP^{2}Ex.

One of the merits of using RSP for this evaluation study is its capability to provide collocated polarimetric and bi-spectral Re retrievals. Thus, the comparison between the RSP bi-spectral and polarimetric retrievals does not need to consider uncertainty resulting from sampling and collocation (a common issue with cross-platform comparisons). Using RSP retrievals alone provides a comparison between the bi-spectral and polarimetric retrieval techniques. The RSP polarimetric retrievals have been examined in other field campaigns, showing good agreement of better than 1 μm compared to in situ measurements in stratocumulus cloud fields (e.g., Alexandrov et al. 2018; Painemal et al. 2021). Here, we extend its evaluation to cumulus cloud fields sampled during CAMP^{2}Ex.

RSP retrieves cloud top heights (CTH) using a multi-angle parallax approach (Sinclair et al. 2017). In addition, a simple cloud mask based on reflectance thresholds is reported, and RSP reports cloud top height retrievals whenever the cloud mask is valid. As we will show in Sect. 4.1, we also make use of valid (non-zero) RSP CTH retrievals to organize cloud properties in cloud elements, where a contiguous set of CTH retrievals is labeled as one cloud element. Means and standard deviations of retrieved quantities are computed for each cloud element. This further allows us to relate cloud properties to cloud macrophysics such as cloud length (characterized by RSP transect length), and cloud top bumpiness (characterized by standard deviation of CTH) at a cloud element level.

2.1.2 SPEC in situ measurements

The Stratton Park Engineering Company (SPEC) provided an array of in situ cloud probes for CAMP^{2}Ex on the NASA P-3 and the SPEC Learjet. During CAMP^{2}Ex, the NASA P-3 often targeted clouds using stacked tracks of in situ cloud legs below and cloud remote sensing legs above the cloud field, while the Learjet provided only in situ

measurements. The Learjet was equipped with in situ instruments only and data from this platform are used to characterize the cloud microphysical properties. For this study, the SPEC in situ instruments include the Fast Forward-Scattering Spectrometer Probe (FFSSP; Brenguier et al. 1998), the Fast Cloud Droplet Probe (FCDP; O'Connor et al. 2008), and the two-Dimensional Stereo (2D-S) probe (Lawson et al. 2006). The FFSSP and FCDP are similar scattering probes that retrieve droplet number concentrations from the forward scattering of a laser impinging on cloud droplets and provide the droplet size distribution in 21 size bins ranging from 1.5 to 50 μm in diameter. The two probes share the same electronics and differ slightly in the design of the probe tips to reduce shattering. The FFSSP was only installed on the Learjet, whereas the FCDP was installed on both the Learjet and P-3. The 2D-S is an optical array probe that uses two orthogonal laser-beams to record images of particles and nominally provides size distributions for diameters ranging from 10 to 3000 μm. We combined the FCDP/FFSSP and 2D-S cloud droplet size distributions for diameters from 1-1280 μm to cover cloud droplet and drizzle sizes. The "breakpoint" to combine the FCDP/FFSSP and 2D-S particle distribution is fixed at 40 μm. Sensitivity tests were carried out using various breakpoints from 25 to 45 μm. We found that the choice of breakpoint does not introduce differences greater than 1 μm in the derived Re for ~90% of the 1 Hz samples used in this study. The FCDP/FFSSP and 2D-S number concentrations are combined at 1 Hz temporal resolution. Only drop size distributions with total number concentrations greater than 10 cm^{-3} and temperatures greater than 0 °C are included in this study following thresholds used to define warm cloud in previous studies (e.g., McFarquhar and Heymsfield 2001). The value of Re from the combined size distributions is calculated as

$$R_e = \frac{\sum_{i=1}^{N} n_i \, r_i^3}{\sum_{i=1}^{N} n_i \, r_i^2},\tag{1}$$

where n_i is the number concentration (#/cm^3) for individual size bins, N is the number of bins, and r_i is the bin-center radius.

The CAMP^{2}Ex data also archives an Re product for full-length cloud passes computed from size distributions summed from all samples belonging to the cloud pass. These size distributions use the FCDP/FFSSP, 2DS, and the High-Volume Precipitation Spectrometer (HVPS, Lawson et al. 1993) to extend the size distribution out to 3-5 mm (in diameter). The multiple probes' size distributions are stitched together using breakpoints that vary from different cloud passes. When compared to our 1 Hz derived Re using only FFSSP/FCDP and 2D-S, our cloud-averaged Re compared favorably to the cloud pass Re stored in the database: The median differences were within 1 μm for both P-3 and Learjet data across all flights, but with a smaller tail in the Re distribution towards larger values – particularly for the Learjet samples, which targeted deeper clouds compared to the P-3. While acknowledging this difference, we used the 1 Hz derived Re from the FFSSP/FCDP and 2D-S since it has a horizontal resolution similar to RSP retrievals at 1.2 Hz. The effects of precipitation on our understanding of RSP bi-spectral and polarimetric Re retrievals are examined here using coincident APR-3 airborne radar data discussed below.

2.1.3 Ancillary data

Apart from the RSP, other remote sensing instruments onboard the P-3 platform provided information about the sampled cloud fields and the surrounding environment that may influence retrieval accuracy. For instance, cirrus above the aircraft can lead to large biases in the bi-spectral retrieved cloud properties as their absorbing effect is not

225 modelled in the retrieval (e.g., Chang and Li 2005). To identify the presence of above-aircraft cirrus, we utilize the measurements from SPN-S (airborne prototype spectral Sunshine Pyranometer, Norgren et al. 2022). SPN-S was mounted on top of the P-3 for measuring downwelling spectral total and diffuse irradiances at wavelengths ranging from 380 to 1000 nm. We derived direct beam transmittances at 860 nm with the assumption that the solar direct-beam is attenuated as prescribed by the Lambert-Beer law. Proper plane attitude adjustment has been applied to the

230 SPN-S data (Bannerhr and Glover, 1991). By collocating the SPN-S transmittance with the cloud retrievals from the Advanced Himawari Imager (AHI) (temporal difference < 10 min and spatial difference < 5 km), we found that the collocated samples have a SPN-S transmittance of less than 0.95 when the AHI cloud phase flag indicates cirrus clouds. Thus, a direct beam transmittance of 0.95 is used to filter out possible above aircraft cirrus contamination.

The Airborne Third Generation Precipitation Radar (APR-3) is used to detect in-cloud drizzle in this study. The

235 APR-3 is a Doppler, dual-polarization radar system operating at three frequencies (13, 35, and 94 GHz). It was mounted looking downward from the P-3 and performed cross-track scans, which covered a swath that is within the $\pm25°$ scan range. The 94 GHz channel's sensitivity to cloud liquid water has led to many studies using it to detect drizzle (e.g., Tanelli et al. 2008; Dzambo et al. 2019; Lebsock and L'Ecuyer 2011). In our analysis, we discovered that Version 2.3 of the APR-3 CAMP^{2}Ex data contained numerous segments containing calibration errors that showed

240 up as large along-track discontinuities in the background noise. This affected about 10% of the total APR-3 data and was therefore removed in our analysis.

The High Spectral Resolution Lidar (HSRL-2, Burton et al. 2018) is a three wavelength lidar that makes measurements of the atmosphere at 355 nm, 532 nm and 1064 nm. It retrieves CTH, and aerosol properties such as extinction coefficient, backscatter and AOD. In our analysis, we take advantage of HSRL-2's capability of providing

245 high resolution CTH at 2 Hz, to supplement RSP in providing cloud macrophysics characteristics of the CAMP^{2}Ex sampled clouds. As we will show in Sect. 4.2.1, we also use HSRL-2 2 Hz CTH to investigate clear sky contamination for the RSP cloud element analysis.

All the instruments on the P-3 platform were temporally synchronized to the meteorological and navigation information provided by the National Suborbital Research Center (NSRC).

250 Compared to past field campaigns, one advantage of CAMP^{2}Ex is the availability of the continuous monitoring from the Advanced Himawari Imager (AHI) on the Himawari-8 geostationary satellite. AHI provides moderate resolution (1 km) reflectances over the entire CAMP^{2}Ex region at 10-minute intervals. This is important for post-campaign data processing since it provides a continuous view of a cloud field's evolution through each research flight.

2.2 MODIS cloud retrievals

255 The main goal of this study is to evaluate and understand the performance of bi-spectral *Re* during CAMP^{2}Ex, including those retrieved by satellites. The satellite *Re* retrievals in this study come from MODIS onboard the Terra satellite. Terra is in a sun-synchronous orbit and has an equator crossing time at 10:30 AM. The *Re* retrieved from the Terra MODIS represents the longest, single-platform, global record of *Re*. In our analysis, we used MODIS Collection 6.1 Level-2 Cloud Products at 1 km resolution (MOD06 V6.1; Platnick et al. 2017). For *Re* and COT, only the standard

260 product from fully cloudy pixels were included, thus excluding partially cloudy pixels. Only liquid water clouds were

considered based on the cloud phase flag provided in the MOD06 product. Only MODIS granules that overlapped with the CAMP²Ex sampling regions during individual P-3 research flights are included. In this analysis, we focus on the Re and COT retrieved using the 0.86 μm and 2.1 μm channel since it is the most widely used and RSP has a similar channel at 2.26 μm. Some recent studies have discussed the validity of comparing the MODIS 2.1 μm channel to the 265   2.26 μm channel from VIIRS, AHI and RSP (e.g., Platnick et al. 2020; Zhuge et al. 2021). It was pointed out that the inconsistency in the spectral response function of the two wavelengths can lead to differences of ~1-2 μm between the Re derived from the two wavelengths, which is much smaller than the Re bias estimates of up to 10 μm reported in Fu et al. (2019). We also examined the MODIS Re product derived using its 3.7 μm channel and found the differences between the Re products derived from MODIS 2.1 μm and 3.7 μm channels to be consistent with what was reported 270   in previous studies (e.g., Zhang and Platnick 2011; Fu et al. 2019). ~~So~~ Thus they are not included in the figures and tables in the following sections. However, we provide a brief summary of these differences at the end of Section 4.3.

2.3 Bias-adjusted MODIS cloud retrievals

The MODIS Re bias estimates presented in Fu et al. (2019) are also evaluated by comparing against the CAMP²Ex dataset. As a continuation of Liang et al. (2015), Fu et al. (2019) fused MISR L1B radiance data and MODIS L2 cloud 275 Re to retrieve COT at MISR's 9 view angles. Liang et al. (2015) revealed that the COT retrievals show a local minimum around the cloud-bow scattering direction (~140°), and this feature was prominent in multi-year climatologies of MODIS cloud COT values and COT retrieved from MISR. They showed that this minimum is due to an overestimate in the MODIS Re product, and that the value of the climatological Re bias could be estimated by extrapolating the Re correction derived from the cloud-bow feature to retrievals at all scattering angles. The local 280   minimum of COT was prevalent in a multiple-year climatology carefully stratified by scattering angle, latitude and solar zenith angle rather than apparent at a ~1-km pixel resolution within a Level 2 MODIS granule because of large spatial variability in scattering angle, solar zenith angle and cloud heterogeneity within a Level 2 granule. To correct for the Re bias, Fu et al. (2019) used 8 years of MISR and MODIS data, and further stratified by MISR nadir τ and cloud heterogeneity to produce climatology estimates of corrected MODIS Re between 60° N and 60° S globally at 285   2.5° resolution for the months of January and July. In the current study, we apply the July regional correction factors from Fu et al. (2019) at 2.5° to the MODIS L2 granules over the CAMP²Ex domain to better compare with Re derived from other techniques under similar seasonal conditions. This allows one to test the robustness of the correction. The average of the July correction factors over the CAMP²Ex domain is ~ 0.6. The correction factors over this region range from 0.25 to 0.97 depending on latitude, τ and cloud heterogeneity. We are interested in evaluating the capability 290   of regional bias corrections to capture the actual variability at its original resolution (i.e., MODIS 1 km retrieval) as we compare to field measurements from CAMP²Ex.

2.4 Co-location technique

One major challenge for constructing the evaluation framework is the collocation between different platforms. In CAMP²Ex, the P-3 performed both remote sensing and in situ sampling during the same flight; simultaneous sampling 295   from both methods is therefore not possible. Furthermore, CAMP²Ex targeted mostly cumulus and congestus clouds

that have faster evolution and shorter lifetime when compared to stratocumulus clouds. A sawtooth flight pattern commonly used in field campaigns targeting stratocumulus regions (e.g., Curry et al. 2000; Painemal and Zuidema 2011; Witte et al. 2018; McFarquhar et al. 2021; Redemann et al. 2021) was not employed during CAMP²Ex. However, while a strict point to point comparison is not achievable, we adopted the following approach to collocate MODIS, RSP and in situ measurements from a statistical standpoint.

A valid collocation between MODIS and the P-3 occurs based on a spatial and temporal matching criterion. For the case-by-case comparisons presented in Sect. 3.3, all samples within the tightest rectangular box circumscribing the P-3 flight path that fell within a ± 1.5-hour of the MODIS overpass time are included in the comparison. This time window was chosen based on the examination of all the 10-min AHI imagery and forward/nadir videos from the P-3 to maintain a balance between ensuring a significant number of samples and ensuring that the airborne remote sensing and MODIS observe the same cloud features. The sensitivity of our results to tighter temporal windows (e.g., 30-min and 1-hour) was tested and did not alter the patterns observed in our results. Of the 19 P-3 research flights, there are 14 research flights that had successful overlap with Terra-MODIS overpasses (Fig. 1 and Table 1).

When comparing remotely sensed *Re* with in situ derived *Re*, one limitation lies in the simplified representation of clouds in the algorithms. Current passive remote sensing assumes clouds to be homogeneous in both the horizontal and vertical direction, but this representation of clouds is different from reality. In nature, clouds tend to have *Re* profile that increase with height (e.g., McFarquhar et al. 2007; Arabas et al. 2009), although relatively constant in the horizontal direction at a given height level (e.g., Khain et al. 2019; Pinsky and Khain 2020; Zhang et al. 2011). The vertical variability of *Re* is often observed from in situ derived *Re* at various levels throughout a cloud. For remotely sensed *Re*, however, satellite retrieved bi-spectral *Re* is viewed as a vertically weighted *Re* with peak weighting near cloud top (e.g., McFarquhar and Heymsfield 1998; Platnick 2000; Nakajima et al. 2010). For the polarimetric *Re* retrievals, the vertical weighting is more strongly peaked and closer to the cloud top compared to the bi-spectral technique. This is because the polarimetric signature is dominated by single-scattering contributions, with a mean penetration optical depth of ~0.5 and negligible contributions from levels below optical depth ~3 from cloud top (Miller et al. 2018). Thus, to directly compare in situ retrieved *Re* with satellite or airborne remotely sensed *Re*, many studies have used in situ measurements at the cloud top to evaluate satellite *Re* (e.g., Painemal and Zuidema 2011; Witte et al. 2018; Gupta et al. 2022). This requires determining the altitude of cloud tops during the in situ legs, which is simple for stratiform cloud with the aircraft performing sawtooth flight patterns at cloud top but not so for cumulus cloud. Here, we made use of all in situ measurements throughout various levels of the cloud fields. While we know the altitude in which the aircraft penetrated cloud, we do not have coincident measurements of collocated cloud top. We exclude in situ samples for which collocated AHI brightness temperature at 11 μm is below 273 K. This removes deeper convective clouds sampled by the aircrafts that are not observed in the warm clouds sampled by passive remote sensing (i.e., RSP). Since the two airborne platforms are equipped with similar SPEC probes, despite the differences in the platform and sampling, the two in situ datasets serve to complement each other, providing additional information that is key to the evaluation of remotely sensed bi-spectral *Re*. We pay special attention to these sampling issues in our comparison of in situ measured *Re* with remotely sensed *Re*.

3 Results

3.1 General cloud characteristics of CAMP²Ex

We begin by providing an overview of some general cloud characteristics derived using the remote sensing data collected by the P-3 for all the research flights. Only oceanic liquid water clouds are included based on the RSP cloud top liquid index (van Diedenhoven et al. 2012). Cloud segments with cirrus overlying are removed based on SPN-S transmittance < 0.95. Segments where the P-3 was banking (i.e., roll angle > 3° and roll angle difference < 1°) are also removed. Data here are organized into cloud elements. Figures 2(a) and (b) show the probability distribution functions (PDF) and cumulative distribution functions (CDF) for cloud element mean Re and COT, respectively, retrieved from RSP polarimetric and bi-spectral (using the 2260 nm channel) techniques. While the COT distributions among the two techniques are in good agreement, the two Re distributions are quite different: the polarimetric Re distribution mode occurs at ~6 μm, whereas the bi-spectral Re mode occurs at ~12 μm. The median polarimetric Re is 7.0 μm, and the median bi-spectral Re is 16.1 μm. The median COT is 3.5 for the standard RSP COT retrievals and 4.2 for the bi-spectral COT retrievals. Figure 2(c) provides the PDFs of RSP mean CTH and HSRL-2 mean CTH, with HSRL-2 CTH from 2 Hz samples. Similar to past studies that compared RSP CTH with airborne lidar retrieved CTH (e.g., Sinclair et al. 2017), the RSP and HSRL-2 CTH distributions in Fig. 2(c) are in excellent agreement, both showing that ~60% of the cloud elements sampled have mean cloud tops < 1 km. Figures 2(d) and (e) show the PDFs of cloud element transect lengths and clear lengths (between cloud elements) derived from the RSP and HSRL-2 CTH mask. We see that 50% of cloud elements sampled by RSP have transect lengths less than 0.6 km, with a mean length of 1.4 km, while 50% of HSRL-2 derived cloud elements have transect lengths less than 0.5 km, with a mean of 1.3 km. 50% of the clear lengths are less than 1.0 km (mean length of 2.6 km) and 0.8 km (mean length of 1.9km), respectively, derived from RSP and HSRL-2. We note that these clouds sampled by the RSP and HSRL-2 have more numerous small clouds than trade cumuli sampled during INDOEX (the Indian Ocean Experiment, Lelieveld et al. 2001) using a Multi-Channel Radiometer (MCR) and during RICO (Rain in Shallow Cumulus Over the Ocean, Rauber et al. 1997) using ASTER (Advanced Spaceborne Thermal Emission and Reflection Radiometer, Abrams et al. 2000), both of which had 50% of the total cloud fraction contributed by cloud area-equivalent diameters less than 2 km and with about half the amount of clouds (McFarquhar et al. 2004; Zhao and Di Girolamo 2007). Given that the mean cloud area-equivalent diameter is approximately 1.1 to 1.7 times of a random linear transect (e.g., Barron et al. 2020; Romps and Vogelmann 2017), the clouds sampled by RSP and HSRL-2 during CAMP²Ex are much smaller than INDOEX's or RICO's trade cumuli. As such, the 1-km resolution MODIS pixels are expected to have a considerable amount of sub-pixel clouds during CAMP²Ex. We speculate that the reason for the maximum failure rate in MODIS cloud microphysical retrievals occurring over the western tropical Pacific, as reported by Cho et al. (2015), may be the high frequency of small clouds here relative to anywhere else. Finally, Fig. 2(f) shows the PDF and CDF of the derived APR-3 W-band maximum reflectivity within individual RSP cloud elements. The APR-3 W-band maximum reflectivity median is at -9.24 dBZ. Past studies have shown a threshold of W-band column maximum reflectivity of ~ -15 dBZ is associated with the transition from non-drizzle to light drizzle (e.g., Dzambo et al. 2019; Wang and Geerts 2003). From Fig. 2(f), ~20% of the valid APR-3 W-band maximum reflectivity values are less than -15 dBZ, indicating that most of the cloud elements sampled by RSP may have some degree of drizzle somewhere in the cloud.

Overall, Fig. 2 reveals that most clouds observed by the P-3 remote sensors are small, optically thin, and often contained pockets of drizzle somewhere within the cloud. Most of the clouds were low clouds with tops under 2 km.
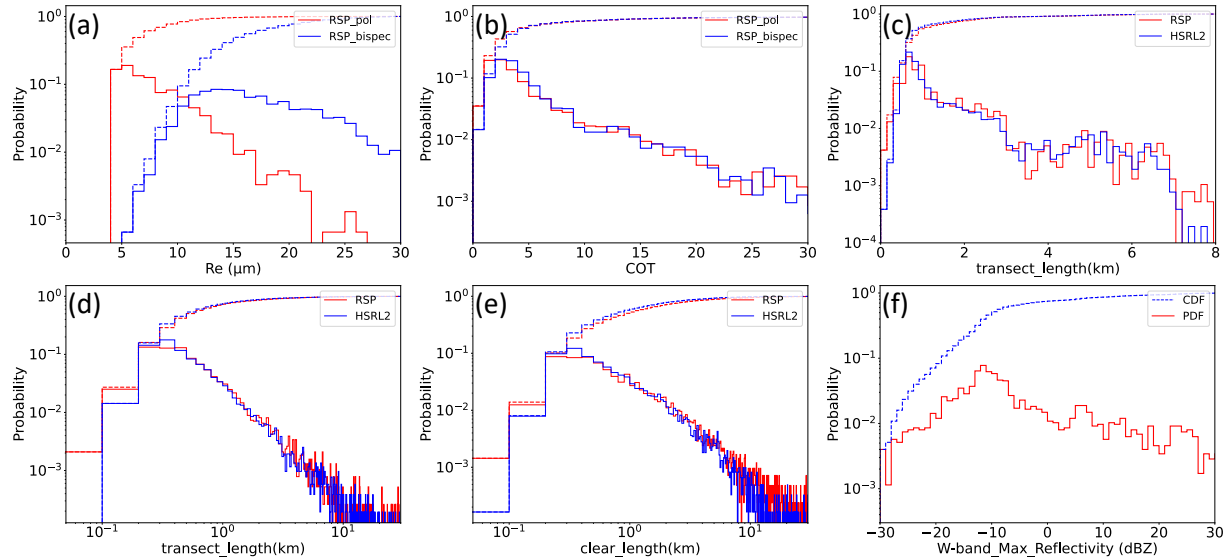
Figure 2. Probability distribution function (PDF, solid line) and cumulative distribution function (CDF, dash line) for cloud element mean values of (a) the RSP polarimetric and bi-spectral *Re,* (b) the RSP polarimetric and bi-spectral COT (c) CTH from RSP and HSRL-2, (d) cloud element transect length from RSP and HSRL-2, (e) clear segment length (between cloud elements) from RSP and HSRL-2, and (f) APR-3 W-band maximum reflectivity within a cloud element, using warm oceanic liquid clouds segments from all P-3 research flights.

3.2 RSP cloud microphysics statistics

The ability to retrieve both collocated polarimetric and bi-spectral *Re* from RSP allows us to compare the performance of the two techniques without further concerns on sampling differences. Figure 3 shows 2-d histograms of RSP polarimetric and bi-spectral *Re*, and *Re* differences (the difference between bi-spectral and polarimetric *Re*) as a function of COT and CTH, using all 1.2 Hz samples passing the above P-3 cirrus filter for oceanic cloud samples during all flights. the differences between bi-spectral COT and ~~cloud bow~~ COT as a function of polarimetric *Re*, and ~~cloud bow~~ COT as a function of CTH are also shown. Several key features are displayed in Fig. 3. Figure 3(a) shows that most of the bi-spectral *Re* are larger than the polarimetric *Re*. A linear regression shows the correlation between the two *Re* is 0.38, with a bias (difference) of 6 μm, and RMSE of 8.2 μm. Figure 3(b) shows a rapid increase in *Re* difference as retrieved optical depths decrease below 5. In other words, the largest *Re* differences are associated with optically thin clouds, which is consistent with the findings from the deployment of RSP during ORACLES (Miller et al. 2020). For CAMP²Ex, the differences between the two *Re* retrievals has a mean of 6.0 μm with a maximum of 26 μm, compared to mean difference of ~1 μm and maximum of 15 μm for ORACLES. The likely reason for the much larger *Re* differences in CAMP²Ex is the greater cloud heterogeneity in the oceanic regions around the Philippines compared to stratocumulus cloud sampled in ORACLES. COT retrievals from the two techniques do not show large differences, as indicated in Fig. 3(c). Most of the COT differences are less than 2 (~20%), which is similar to the results in Miller et al. (2020). Finally, when the *Re* differences are binned by CTH (Fig. 3(d)), the *Re* differences decrease as CTH increases for low to mid-level clouds (CTH < 4km). As seen from Fig. 3(e), COT increases with

395   CTH which would also result in liquid water path increasing with CTH. Beyond 4 km, no clear trend of *Re* difference related to CTH is observed, perhaps because the population is largely alto-clouds as evident in Fig. 3(e).
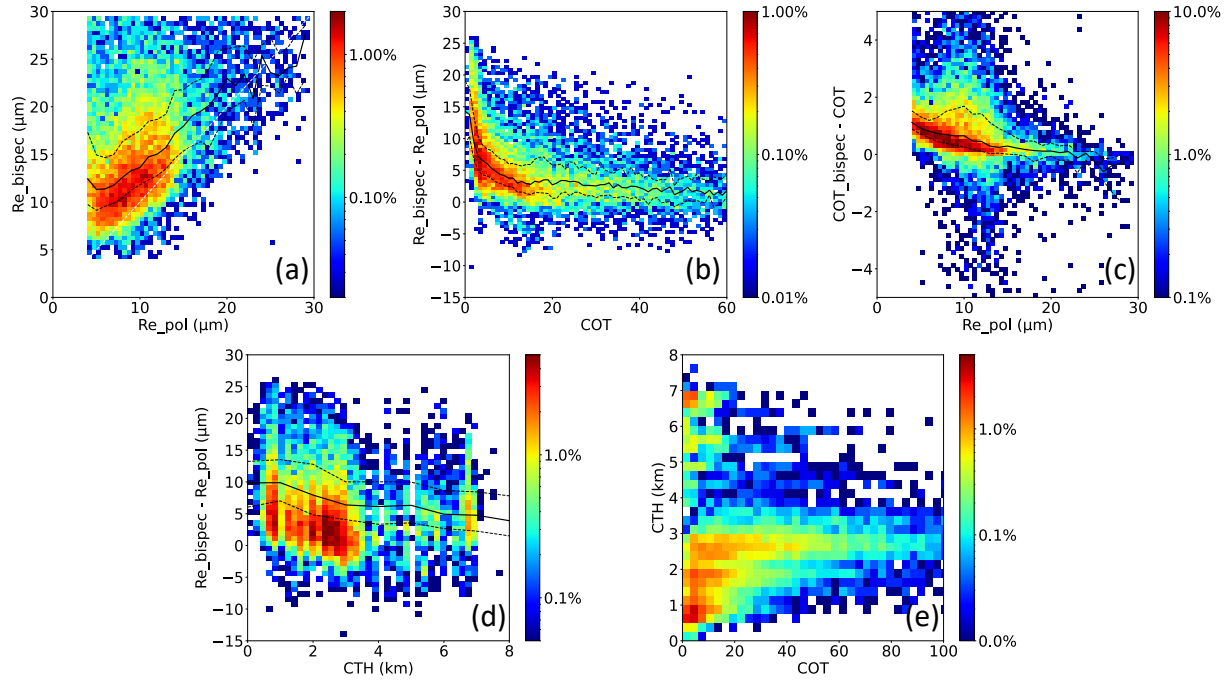
Figure 3. RSP 2-d density histogram of (a) polarimetric *Re* vs. bi-spectral *Re*; (b) RSP COT ~~(cloud bow COT)~~ vs. *Re* difference (bi-spectral *Re* – polarimetric *Re*); (c) polarimetric *Re* vs. COT difference (bi-spectral – cloud bow); (d)
400   CTH vs. *Re* difference (bi-spectral *Re* – polarimetric *Re*); and (e) ~~cloud bow~~RSP COT vs. CTH. Black solid lines in (a) through (d) plot the median with respect to each horizontal bin, black dash lines indicate interquartile.

This comparison indicates that the bi-spectral *Re* are considerably larger than the polarimetric *Re*. However, without further examining the details of the macrophysics and the microphysics of the sampled cloud fields, it is difficult to comment on possible causes for the observed *Re* differences. Therefore, it is necessary to focus on
405   individual cloud fields to study the characteristics of each cloud field (Sect. 3.3), and then relate the observed *Re* differences to other observed properties, such as cloud macrophysics and the presence of drizzle. Possible causes of the differences between the two *Re* retrieval techniques are further explored in Sect. 4.

3.3 Individual case studies

In our analysis above, we examined the general cloud characteristics and RSP bi-spectral and polarimetric
410   retrieval differences over all 19 P-3 RFs from CAMP²Ex. Here we provide a few case studies to illustrate detailed inter-comparisons between remote sensing (satellite and aircraft) and in situ retrievals of *Re* during CAMP²Ex. Cases were selected when there was a good overlap between the sampling of MODIS, RSP and in situ over cirrus-free liquid-phase cloud fields over ocean. Table 2 provides the details of selected cases including the geolocation, MODIS overpass time, selected collocation time period of RSP, and in situ from P-3 and Learjet. For each case, we compare
415   *Re* from RSP, in situ from the P-3 platform, in situ from SPEC Learjet, MODIS, and the bias-adjusted MODIS *Re* of Fu et al. (2019) to evaluate the performance of bi-spectral *Re* against polarimetric *Re* and in situ *Re* measurements.

For a shallow cumuli case from RF17, the collocated hi-resolution ASTER (also onboard Terra) data allow us to highlight the representativeness of MODIS L2 cloud retrievals in sub-pixel cloud fields. In an effort to keep this discussion concise, we discuss only RF02 here, and move additional figures and discussions for the RF07, RF12 and
420   RF17 case studies in Supplemental Materials.

Table 2. Individual case details: Research Flight (RF) designation, approximate domain-center geolocation, MODIS overpass time (UTC), RSP, P-3 in situ and Learjet in situ time periods (UTC), and a brief description of sampled cloud fields.

RF	Domain center lat/lon	MODIS overpass time	RSP time period	P-3 in situ time period	Learjet in situ time period	Features of interest
2	18.5° N, 117° E	8/27/19 3:05	8/27/19 3:36-4:30	8/27/19 3:00-3:30	N/A	Field of shallow to moderate cumuli
7	19° N, 123.5° E	9/9/19 2:34	9/9/19 1:00-2:12	9/9/19 3:00-3:45	9/9/19 1:48-2:18	Isolated cold pool/convective clouds
12	18° N, 125° E	9/22/19 2:03	9/22/19 2:12-3:18	9/22/19 1:50-2:05	9/22/19 1:00-1:42	Moderate convection, cold pool and shallow cumuli
17	20° N, 120° E	10/2/19 2:40	10/2/19 1:55-4:10	10/2/19 1:10-1:50	N/A	Field of small shallow cumuli

3.3.1 27 Aug. 2019 research flight 2

425   During RF02, shallow convection was observed near 18.6° N, 116.9° E, as shown in the MODIS RGB image (Fig. 4(a)) during the Terra overpass at 03:05 UTC. The P-3 first entered the area depicted in Fig. 4(a) around 03:00 UTC on a low altitude leg (~500m) sampling below the shallow cumulus field. Between 03:00 UTC and 03:30 UTC, the P-3 conducted several upward ascents into level legs to sample clouds in situ. Several high-altitude remote sensing legs were flown between 03:30 UTC and 04:30 UTC, sampling along a cumulus cloud line between 17° N to 19° N
430   and 116° E to 117° E as indicated in Fig. 4(a). This cloud field occurred in the vicinity of a larger low-pressure system east of Luzon; some thin cirrus clouds are observed to the east of the sampled clouds. During the 1.5-hour time period, AHI imagery indicated that the shallow convective line retained its overall pattern and distributions, exhibiting consistent cloud top structures of typical broken shallow to moderate cumulus. Cirrus and ice clouds were filtered out from MODIS according to MODIS L2 phase flag. For the P-3 platform, the lower cumuli were mostly not affected by
435   cirrus as seen from the AHI imagery and according to the SPN-s transmittance above the P-3. MODIS Level 2 retrievals show Re ranging from 8 to 30 μm, associated with optically thin to moderately thick COT (1 - 50) and CTH of ~500 m to 4000 m. The RSP bi-spectral Re also shows a range of 8 to 30 μm similar to MODIS. In great contrast, RSP polarimetric Re, bias-adjusted MODIS Re and in situ derived Re from P-3 all suggest a similar range of 5 to 15 μm (with only a few outliers ~20 μm), which is much lower than the bi-spectral Re retrievals. The W-band maximum
440   reflectivity from APR-3 indicates some precipitation in the deeper clouds (CTH > 2 km).
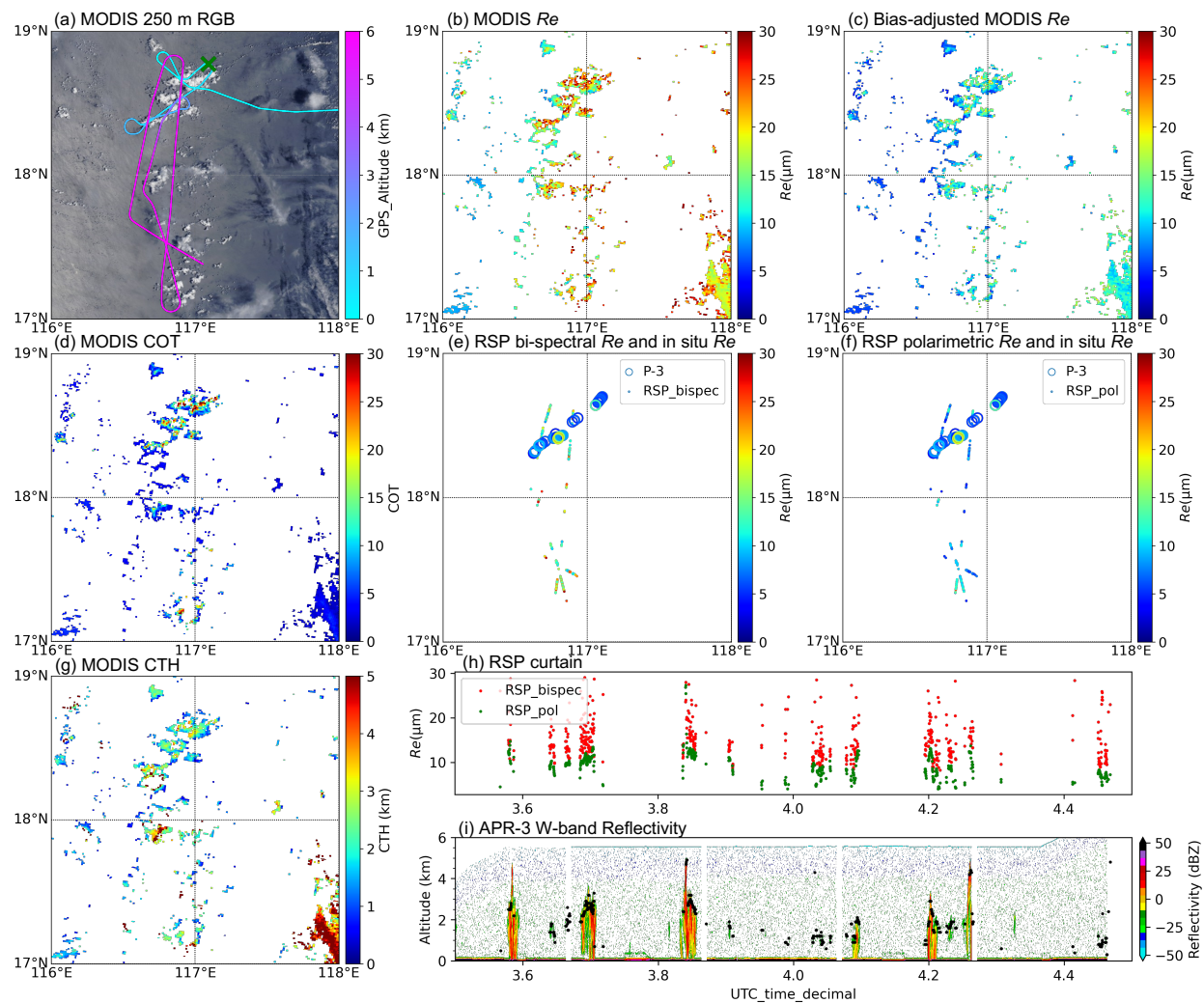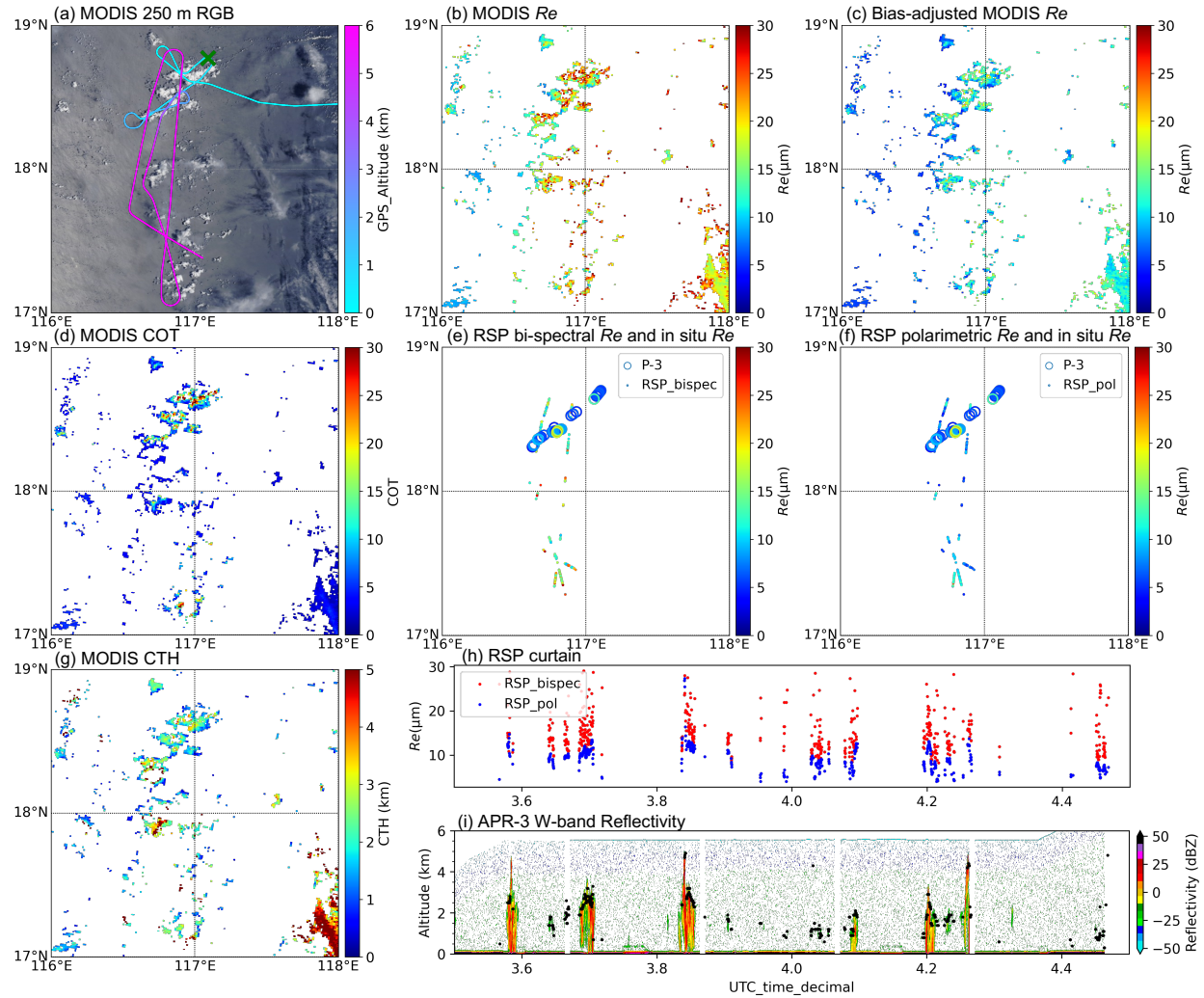
Figure 4. (a) MODIS RGB reflectance at 3:05UTC on 27 Aug. 2019. Color bar indicates P-3 altitude and flight track within ±1.5 hours of MODIS overpass time. Green cross indicates P-3 location at MODIS overpass time. (b) MODIS Level-2 1 km *Re* retrievals from 2.1 μm channel. (c) MODIS Level-2 1 km bias-adjusted *Re* retrievals from 2.1 μm channel after applying Fu et al. (2019) correction factors. (d) MODIS Level-2 1 km COT from 2.1 μm channel. (e) RSP bi-spectral *Re* retrievals from 2.26 μm channel. In situ *Re* from P-3 is displayed in circles. (f) RSP polarimetric *Re* retrievals from 0.86 μm channel. In situ from P-3 is displayed in circles. (g) MODIS Level-2 1 km CTH retrievals. (h) RSP *Re* curtain between 03:30 UTC and 04:30 UTC. (i) APR-3 W-band reflectivity and RSP CTH (black dots) between 03:30UTC and 04:30UTC.

RSP bi-spectral and polarimetric *Re* have the same sampling, as does MODIS *Re* and the MODIS bias-adjusted *Re*. So, they are directly comparable. But a direct pixel-to-pixel comparison between MODIS, RSP and in situ sampled *Re* values is essentially impossible since they are not coincident in space and time. Still, the samples were collected in a fairly small space and time window over which little overall change in the cloud field occurs as indicated by AHI imagery. We sorted the *Re* retrievals into 250 m CTH bins. The *Re* mean and standard deviation are computed for each height bin as a means of comparing remote sensing techniques' ability to capture the variations of *Re* with CTH, which is important when using the data for understanding cloud processes. Since the tops of cumulus clouds sampled in situ are hard to determine, the platform altitude was used for in situ sampling, noting that these in situ derived *Re* are in-cloud measurements rather than a vertically weighted near cloud top *Re* as obtained from remote sensing. While

460 acknowledging the different sensitivity to cloud exterior and in-cloud microphysics for these different techniques, observations and simulations have shown, for shallow cumulus clouds that low variation of *Re* (~10%) exist between the exterior and interior of clouds at a given altitude (e.g., Khain et al. 2019; Gerber et al. 2008). Thus, we primarily focus on accounting for the systematic variation with altitude. To do this, we binned *Re* retrievals from all 5 techniques (P-3 in situ, RSP polarimetric, RSP bi-spectral, MODIS bi-spectral, and bias-adjusted MODIS) separately as a

465 function of binned CTH/altitudes. The results for the RF02 case are given in Fig. 5. All 5 techniques indicated an overall pattern of increasing *Re* with height. One prominent feature of Fig. 5 is that for mid to low level cloud tops (below 3.5 km), the P-3 in situ (FCDP and 2D-S), RSP-polarimetric and bias-adjusted MODIS *Re* all indicate an increasing *Re* profile from ~7 μm to ~15 μm in the mean values. Thus, despite the differences in sampling and retrieval technique, the three are very consistent; the mean difference between the three *Re* profiles (Table 3) are all within 2

470 μm. The bi-spectral *Re* from RSP and MODIS, however, shows much larger values than the other three techniques, with increasing *Re* profiles from ~13 to ~22 μm. Thus, despite sampling and resolution differences, these two bi-spectral products are consistent among themselves with the RSP bi-spectral *Re* ~3 μm smaller than that from MODIS. The bi-spectral *Re* from MODIS and RSP also show much greater *Re* variability at each height level (as seen from the horizontal whiskers), compared to RSP-polarimetric, in situ and bias-adjusted MODIS *Re*. For CTH below ~1.3 km,

475 RSP bi-spectral *Re* suggests a decreasing *Re* profile, essentially opposite of other techniques. At higher altitudes, existence of drizzle tends to result in higher *Re* values with larger variability for both RSP polarimetric and bi-spectral *Re* retrievals. The APR-3 and RSP curtains in Fig. 4 also confirms the correlation between drizzle and larger *Re* values for both techniques. At ~3.5 km, in situ derived *Re* indicated values of 13 – 20 μm, as it penetrated a convective cloud whose tops were higher than the P-3 by several hundred meters and visually appeared to be optically thick, as indicated

480 by the P-3 forward video just before cloud penetration. Splashing of precipitation on the P-3 windshield was also evident from the forward video. Apart from sampling differences, some of the variability between in situ *Re* and the remotely sensed *Re* may also be due to entrainment and mixing (e.g., Gerber et al. 2008).
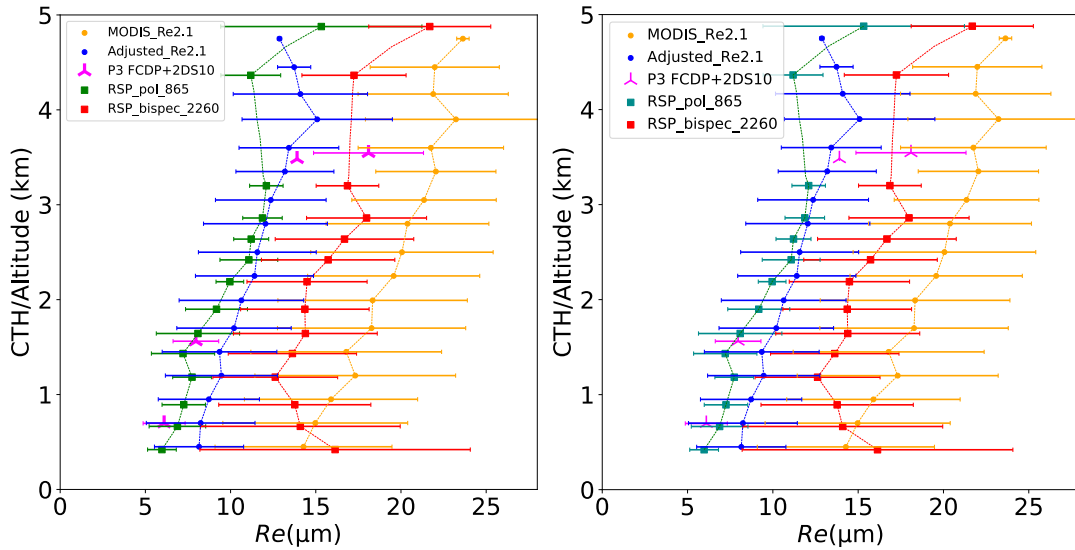
Figure 5. *Re* profile (mean *Re* vs. mean height) of vertically binned MODIS *Re*, bias-adjusted MODIS *Re* (after applying Fu et al. (2019) correction factors), RSP polarimetric *Re*, RSP bi-spectral *Re* and P-3 in-situ derived *Re* for the RF02 case. Horizontal whiskers indicate standard deviation of data within each 250m altitude bin.

3.3.2 Summary and discussion of cases studies

The analysis and discussion of RF07, RF~~0~~12, and RF17 presented in Supplemental Materials follows the ~~above~~ figures and discussion given above for RF02. Table 3 summarizes the mean difference between the RSP polarimetric *Re* with the other techniques for these cases. At lower altitudes, the Learjet and P-3 in situ and RSP polarimetric *Re* are in good agreement. While acknowledging the definition of *Re* is different for remote sensing retrievals and in situ measurements, the overall good agreement between polarimetric and in situ *Re* should bring more confidence in the performance of polarimetric *Re* retrievals in cumulus cloud fields. In all comparison cases, RSP polarimetric *Re* also agrees well with the MODIS bias-adjusted *Re*, despite the resolution and sampling differences between the two. Finally, both the RSP bi-spectral and MODIS *Re* show good agreement with each other, but with the overall largest *Re* values among all techniques. The distinct separation between bi-spectral *Re* and *Re* from all other techniques implies an overestimate in bi-spectral *Re* for cumulus clouds regions; the mean *Re* differences of ~5 - 10 μm in the individual cases matching with the estimates of ~ 6 - 9 μm bias in 2.1 channel MODIS *Re* found by Fu et al. (2019).

The impact of drizzle on *Re* from these case studies ~~were~~ was evident in remotely sensed and in situ observations. Direct comparison between in situ and remote sensing in deeper clouds containing drizzle was hampered by the fact that the in situ samples containing drizzle and large *Re* occurred at locations that were not close to cloud top according to the aircraft forward video. We therefore take a more extensive examination of the impact of drizzle on our comparison of bi-spectral and polarimetric retrievals in Sect. 4.2.2 using APR-3.

As mentioned in Sect. 2.2, we acknowledge the channel differences between the MODIS 2.1 μm and RSP 2.26 μm *Re* retrievals, so we do not expect the *Re* retrieved from MODIS and RSP bi-spectral to have the exact same bias. In our analysis, other contributing factors that may impact the differences between RSP 2.26 μm bi-spectral *Re* and MODIS 2.1 μm *Re* include (1) sampling differences (2) channel differences in the face of vertical and horizontal variations in cloud optical properties, and (3) pixel size difference in the face of 3-D variations. Despite these factors, the RSP 2.26 μm bi-spectral *Re* and MODIS 2.1 μm *Re* have very similar behavior, exhibiting a large positive bias and much greater variability in *Re* relative to the other techniques.

Table 3. Mean bias (difference) between RSP polarimetric with the other techniques for the four cases studies.

mean bias wrt. RSP Polarimetric *Re* (μm)	RF02	RF07	RF12	RF17
RSP bi-spectral *Re*	6.0	5.0	6.0	9.8
MODIS *Re*	9.2	6.1	7.2	8.3
MODIS-Bias-adjusted *Re*	1.4	1.6	1.6	2.6
P-3 in situ *Re*	0.5	0.2	0.8	0.1
LJ in situ *Re*	N/A	9.4 (all) 0.8 (below 2 km)	1.1	N/A

3.3.3 A brief look at representativeness of MODIS retrievals with ASTER

As indicated in Fig. 2, CAMP²Ex samples contain lots of small clouds, and brings into question issues of sub-pixel clouds on MODIS retrievals and their representativeness in cloud climatologies. Here we use RF17 to illustrate a few points. RF17 sampled a field of small, shallow cumuli that appear very different than the previous cases. The most prominent feature for this case is the abundance of small broken cumulus clouds in this domain (Fig. 6(a)). On October 2nd around 01:00UTC, the P-3 platform entered the region at around 1.5 km altitude and then descended to ~100 m above sea level to begin in situ measurements below cloud base and at various levels within clouds. Around 02:00 UTC, the P-3 started climbing from 1 km to 5 km altitude to perform remote sensing sampling, with long stretches of straight legs as shown in Fig. 6(a). The aircraft exited the region around 04:30UTC. A Terra overpass took place at 02:40UTC. The MODIS and ASTER imagery indicate that clouds in this case were mostly very shallow, small cumuli. To better demonstrate the representativeness problem with MODIS retrievals in this common type of cloud field, we overlayed the MODIS 1 km resolution *Re* retrievals over the MODIS 250 m RGB imagery (Fig. 6(a)) and ASTER 15 m radiances (Fig. 6(b)) for the box region highlighted in red in Fig. 6(a).

Figure 6(a) shows that while there are numerous very small broken cumulus clouds in the scene, the MODIS Level 2 *Re* only reported a handful of pixels having successful retrievals. For the successful MODIS *Re* retrievals shown in Fig. 6(b), the estimated cloud fraction from ASTER 15 m imagery range from ~0.25 to 0.62. It clearly shows that these small cumuli are sub-pixel for MODIS Level 2 retrievals with cloud variability that cannot be resolved by MODIS. It is expected that this unresolved variability leads to biases in MODIS retrieved *Re*, which we further investigate in Sect. 4.2. The MODIS *Re* retrievals (Fig. 6(a) and Fig. 6(d)) and RSP bi-spectral retrievals (Fig 6(c)) both suggest *Re* values in the range of 6 to 30 μm (median *Re* value of 14.0 μm for MODIS *Re* and median *Re* value of 12.0 μm for RSP bi-spectral *Re*). RSP polarimetric *Re*, however, shows much smaller values of 4 to 7 μm (median *Re* value of 5.3 μm) that also agrees well with the P-3 in situ *Re* (median *Re* value of 6.1μm). Similar to Fig. 5, *Re* retrievals from the different techniques binned by CTH/altitude for the RF17 case is included in the Supplemental Materials (Fig. S6).

While not shown, many clouds in the scene are correctly identified by MODIS as partly cloudy pixels (PCL) and excluded from the standard *Re* product analyzed here. We examined MODIS PCL retrieved *Re* within the domain in Fig. 68(a), the MODIS PCL *Re* retrievals revealed that ~~most of that~~ most of the *Re* were in the 10 to 30 μm range, with a median value of 18.5 μm, which is 4.5 μm larger compared to the standard MODIS *Re*. This is mostly due to MODIS not being able to resolve the sub-pixel variability, and the low sub-pixel cloud fraction would lead to erroneously larger *Re* values. Some failed retrievals may also be attributed to the finite range of the bi-spectral look-up table (LUT). For example, Cho et al. (2015) showed that failed retrievals in the MODIS product would occur whenever the retrievals fall outside the LUT range, and this failure rate can be as high as 40% in the Southeast Asia oceanic region. This questions the validity of the representativeness of long-term MODIS climatologies for regions dominated by small cumulus cloud fields.
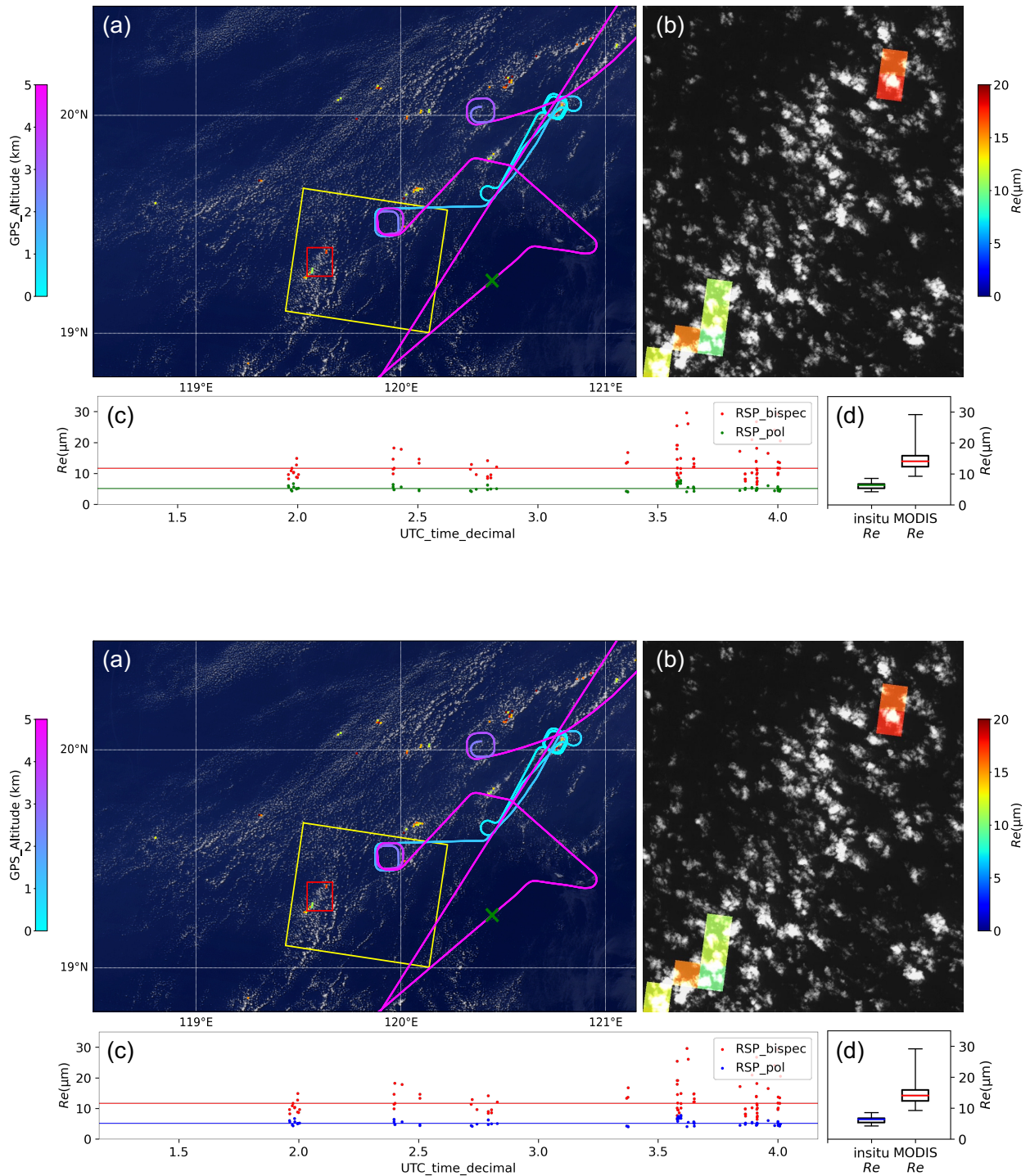
Figure 6. (a) MODIS 250 m RGB Reflectance at MODIS overpass (2:40UTC) overlayed by MODIS Level 2 liquid Re retrievals, RF17 P-3 flight path within 1.5 hours of MODIS overpass color-coded by altitude. The green cross indicates P-3 position at MODIS overpass time. Yellow box indicates outline of the collocated ASTER 15 m granule. Red box indicates outline of the zoom-in view. (b) zoom-in view of ASTER 15 m resolution 3N channel radiance, overlayed by MODIS Level 2 liquid Re retrievals. (c) scatter plot of RSP polarimetric and bi-spectral Re retrievals

within 1.5 hours of MODIS overpass time, the ~~green~~ blue and red line indicate the median value for the RSP polarimetric and bi-spectral *Re* retrievals, respectively. (d) box plots of MODIS *Re* retrievals shown in (a) and P-3 in situ derived *Re* within 1.5 hours of MODIS overpass time. Line in the box indicates median *Re* value.

4 Relating *Re* bias to 3-D factors, sub-pixel heterogeneity and drizzle

Since the largest (i.e., > 5 μm) observed *Re* bias between the bi-spectral and polarimetric technique tends to occur for small retrieved optical thickness (COT <5, Fig. 3(b)), it is especially important to consider the uncertainties in the retrieval process that can affect the bi-spectral retrieval, even when the core assumptions of 1-D radiative transfer are met. Sources of uncertainty include instrument calibration, atmospheric correction, surface Bi-directional Reflectance Distribution Function (BRDF) and assumed size distribution shape as well as retrieval logic. These uncertainties are derived for MODIS in Platnick et al. (2004), and globally validated for COT retrievals of oceanic liquid water clouds in the limit of homogeneous clouds in Di Girolamo et al. (2010). Still, even in the case of ideal simulated 1-D retrievals, retrieved *Re* values can be biased high due to the presence of multiple *Re* solutions and limitations of lookup table interpolation for low optical depth (Miller et al. 2018). However, these large *Re* retrievals are much more frequent in our data (e.g., Fig. 3(b)) than can be reasonably explained by these sources of uncertainty, as discussed below.

For MODIS, the uncertainty in retrieved *Re* can be significant (16-30%) for (COT < 5) (Platnick et al. 2017). Similar uncertainties can be anticipated for RSP, since RSP has a calibration uncertainty of 3% (Knobelspiesse et al. 2019) that is similar to MODIS. Even in the worst case that all uncertainties are systematic across the field campaign period, these uncertainties are much smaller than the factor of two differences observed between RSP polarimetric and bi-spectral *Re* with COT < 5. This indicates that other retrieval assumptions should be investigated to understand the cause of the observed differences between *Re* retrieval techniques.

The literature contains extended discussions relating passive cloud retrieval bias in COT and *Re* to the impact of sub-pixel heterogeneity and other 3-D effects (e.g., Marshak et al. 2006; Zhang and Platnick 2011; Zinner et al. 2010; Zhang et al. 2012; Zhang et al. 2016), sun-view geometry (e.g., Loeb and Davies 1996; Várnai and Davies 1999; Liang and Di Girolamo 2013; Grosvenor and Wood, 2014), and the presence of drizzle (e.g., Zhang et al. 2012; Ahn et al. 2018). In this section, we test the hypothesis that retrieval errors from 3-D effects contribute to measurable bias in *Re* retrievals from CAMP[2]Ex dataset. To facilitate our investigation, we used a cloud element labelling technique based on RSP L2 cloud retrievals, where a cloud element is defined as a region with contiguous CTH retrievals. We then provide statistics of cloud microphysics and macrophysics for each cloud element. We use cloud macrophysical properties (e.g., cloud size, cloud top bumpiness, CTH) and solar zenith angle to relate to 3-D radiative effects and test the sensitivity of the *Re* bias to these factors (Sect. 4.2). We also looked at the impact of drizzle on *Re* bias and found no apparent relationship between the two (details in Sect. 4.2.2).

4.1 RSP cloud element analysis

The cloud element labelling technique was developed using the RSP CTH retrievals. A contiguous set of CTH retrievals are counted as one cloud element. Places with no-retrievals between the cloud elements are labeled as "clear" segments. For each cloud element, means and standard deviations of cloud properties (*Re*, ~~optical depth~~COT, CTH) are calculated along with the cloud elements' horizontal length. This method allows one to further relate the RSP retrieved cloud properties to quantities such as the standard deviation of CTHs and cloud horizontal length, which can

590   serve as proxies for cloud top bumpiness and cloud size to further investigate the sensitivity of *Re* retrievals to these factors. When developing the cloud element labelling technique, we compared the cloud elements derived using RSP CTHs with that derived from HSRL-2 CTHs (Fig. 2(c)). While the two CTHs showed very similar results, we chose to use RSP since *Re* and COT are tied directly to RSP sampling.

      This cloud element analysis was implemented for all research flights with good cloud sampling segments (number

595   of cloud elements > 3), without further consideration for MODIS or in situ collocations. Table 4 lists the 12 research flights and time periods used in our analysis. Fig. 7 shows mean *Re* values for each cloud element as a function of its mean CTH, with whiskers representing the standard deviations of *Re* and CTH for the cloud element. Each cloud element is color-coded by its cloud transect length. A prominent feature in Fig. 7 is the high degree of correlation between RSP polarimetric *Re* and CTH means (linear correlation coefficient, r, of 0.64 averaged across all 12 cases),

600   compared to the correlation between RSP bi-spectral *Re* and CTH means (r = 0.18 averaged across all 12 cases). The variability of bi-spectral *Re* is also much larger than that of polarimetric *Re* across all CTH levels, particularly for the lower levels (below 2 km). Colors also indicate that lower clouds are more often found with smaller lengths (less than 5 km, and often less than 1 km), indicating that low clouds are mostly very small cumuli. Figure 7 also shows that higher clouds often have higher CTH standard deviations, indicating bumpier cloud tops. Overall, the bi-spectral *Re*

605   values are much larger than the polarimetric *Re* values across all CTH ranges. Across all 12 flights, the mean *Re* difference between the bi-spectral and the polarimetric *Re* is 11 µm.

Table 4. The time periods from 12 Research Flights used to construct the analysis of Fig. 7.

P-3 Flight Date by UTC start	RSP Time period (UTC)
8/27/2019 RF02	8/27/19 3:30-4:30
8/30/2019 RF04	8/31/19 2:10-3:30
9/8/2019 RF07	9/9/19 1:00-2:12
9/13/2019 RF08	9/14/19 0:10-1:00
9/15/2019 RF09	9/16/19 3:00-4:00
9/16/2019 RF10	9/16/19 23:30-25:00
9/21/2019 RF12	9/22/19 2:12-5:40
9/23/2019 RF13	9/24/19 1:00-3:50
9/25/2019 RF14	9/25/19 3:30-5:30
9/27/2019 RF15	9/28/19 1:50-3:50
10/1/2019 RF17	10/2/19 1:50-4:30
10/5/2019 RF19	10/5/19 2:00-4:30
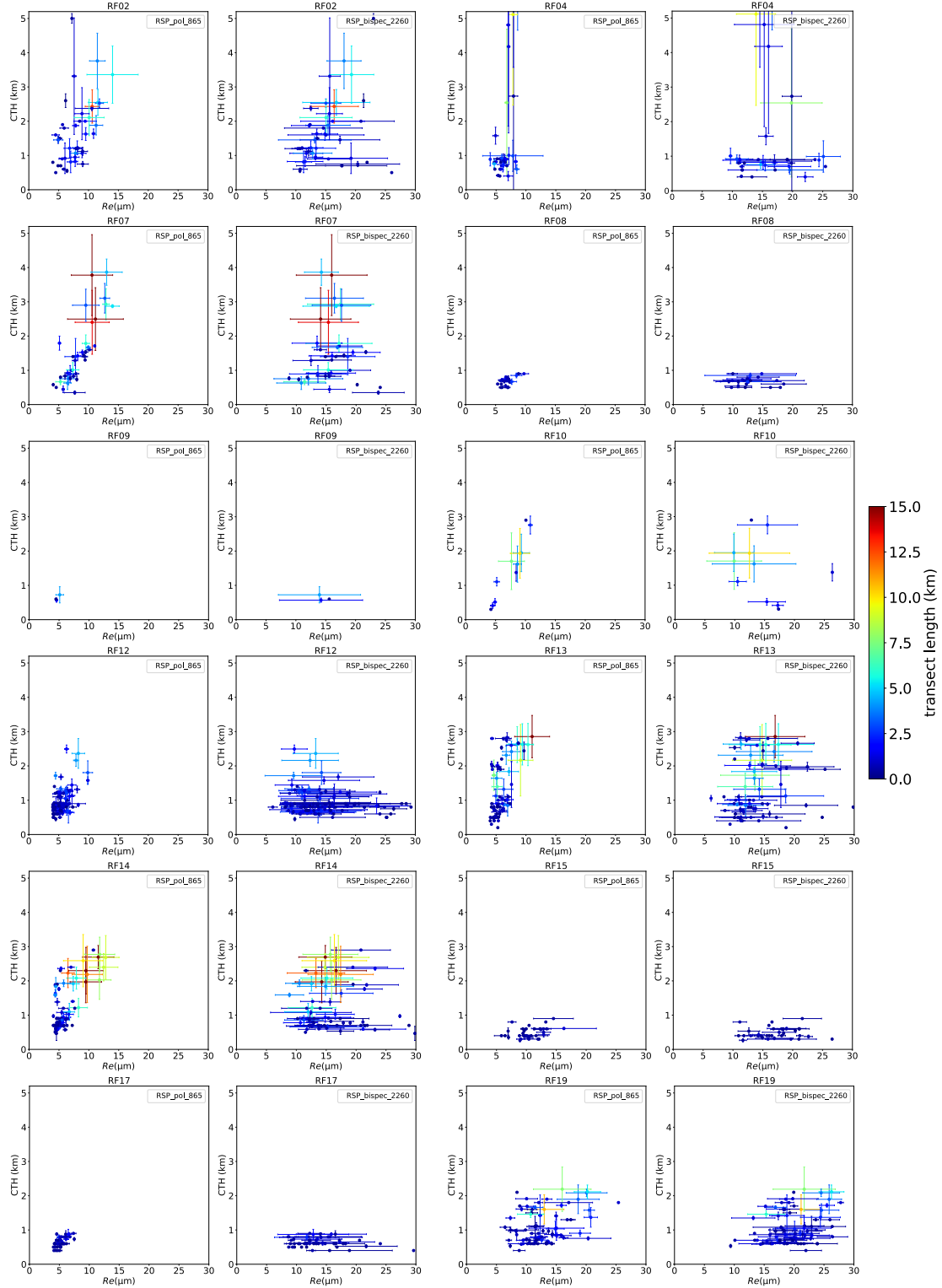
Figure 7. RSP Cloud element mean *Re* vs. mean CTH for from 12 research flights with good RSP sampling of warm cumulus and congestus clouds. The dots represent the mean *Re* value vs. mean CTH of each cloud element, the whiskers indicate standard deviations of *Re* and CTH for each cloud element. Cloud elements are color-coded by their horizontal transect lengths.

4.2 Sensitivity of *Re* retrieval bias to potential factors

In this section, the RSP cloud element statistics throughout the entire CAMP²Ex mission are used to investigate the impact of various potential factors to the observed *Re* differences between RSP polarimetric and bi-spectral retrievals. The factors investigated include COT, cloud size, cloud top bumpiness, sub-pixel heterogeneity, SZA, and drizzle. In reality, the impacts of these factors are often intertwined. For example, clouds with smaller lengths are also shallower and optically thinner. Deeper clouds may also have larger lengths and increased likelihood of drizzle. While it is not possible to fully isolate the impact from each individual factor, we will focus our discussion primarily within the scope of 3-D radiative effects, sub-pixel heterogeneity and drizzle.

4.2.1 3-D radiative effects and sub-pixel heterogeneity

Cloud optical thickness and cloud size

Figure 8(a) shows the differences between the cloud element mean polarimetric *Re* and bi-spectral *Re* retrievals organized as a function of cloud optical thickness. A sharp decrease of *Re* differences (bi-spectral − polarimetric) from ~25 μm to ~8 μm (maximum *Re* difference) is observed with increasing COT up to 9. This difference tapers off to a value of roughly 4 μm for larger COT. This pattern is similar to Fig. 5(a) in Marshak et al. (2006), where they used 3-D LES simulations to discuss the radiative effects of cloud's 3-D structure in 1-D *Re* retrievals from the bi-spectral technique. Marshak et al. (2006) concluded that in cumulus cloud fields, shadowing effects (defined as when the measured reflectance is lower than its 1-D plane parallel equivalent reflectance) dominates over illumination effects (measured reflectance is higher than its 1-D plane parallel equivalent reflectance), and lead to an overestimate in retrieved 1-D *Re*. Vant-Hull et al. (2007) studied the impact of scattering angle on cumulus clouds to find that far from the backscatter direction (where shadowing effects dominate), 3-D cloud structures would lead to overestimates in the 1-D bi-spectral *Re* retrievals. However, near the backscatter viewing geometry (where illumination effects dominate), the opposite is true. These effects in cumuliform cloud fields so far have been only studied through simulations. Since RSP bi-spectral retrievals were never taken close to the backscatter direction, the expectation is an overall overestimate of retrieved *Re* from the bi-spectral technique. If we assume the RSP polarimetric *Re* as the true *Re* (given how well it compared with in situ derived *Re* in Sect. 3.3), Fig. 8(a) suggests that in broken cumulus scenes (typical in CAMP²Ex) large overestimates in bi-spectral *Re* dominate, being consistent with these earlier studies that were based on simulations. But differences do exist. For example, we observe fewer negative values of scattered *Re* differences in Fig. 8(a) compared to Fig. 5(a) of Marshak et al. (2006). This may be due to different sun-view geometries, cloud structures, and cloud microphysics between RSP retrievals in CAMP²Ex and the simulations in Marshak et al. (2006).

Figure 8(b) shows the relationships between the *Re* differences, COT and the cloud element's transect length as measured by RSP. We see that cloud elements with the largest *Re* differences (up to 25 μm) tend to be associated with the smallest transect lengths (< 1 km) and smallest retrieved COT. As the transect length increases to 3 - 5 km, the large *Re* differences drop rapidly, showing no further dependence on transect length. Smaller transect lengths are strongly associated with smaller clouds, with mean cloud area-equivalent diameters ~1.1 to 1.7 times larger than the mean of random linear transects though fields of cumuli (e.g., Barron et al. 2020; Romps and Vogelmann 2017). Fig.

650   8(b) reveals that clouds with the smallest sizes have the largest *Re* differences between the two techniques. These smaller clouds are associated with smaller retrieved COT. These 1-D retrieved COT may be biased low by 3-D effects, such as shadowing and leakage of photons out the side of clouds (e.g., Marshak et al. 2006). From Fig. 8(b), it is safe to conclude that RSP cloud element analysis reveals that the largest *Re* differences are associated with clouds that are optically thin and small in horizontal size.

655
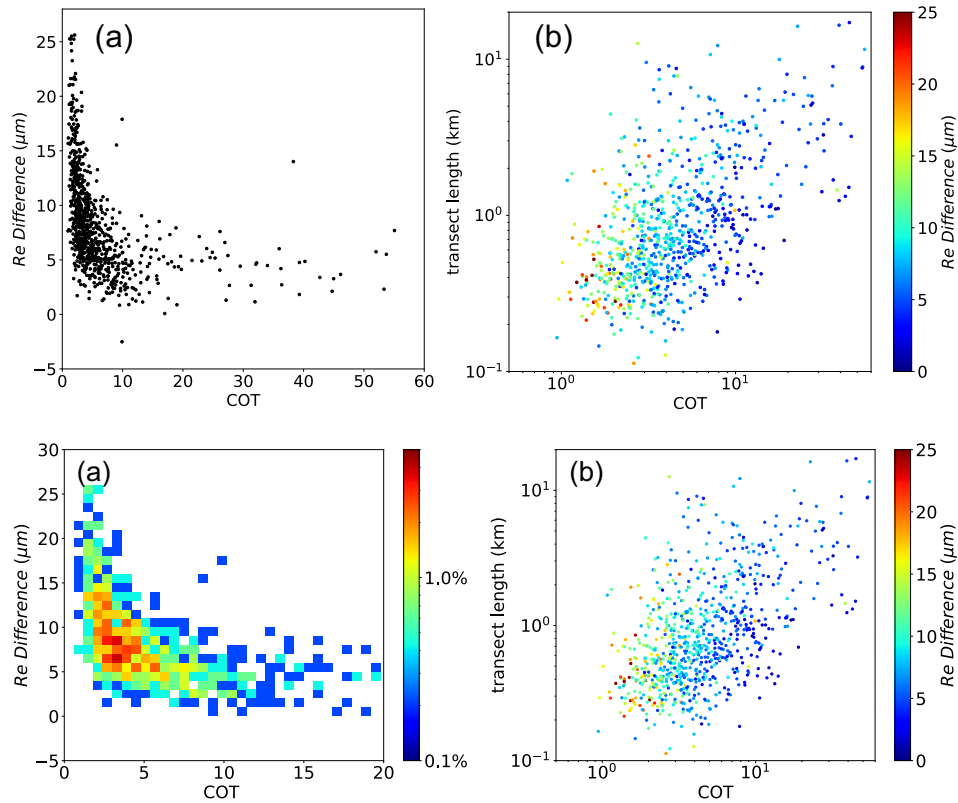
Figure 8. (a) Density plot of cloud element mean *Re* difference (bi-spectral – polarimetric *Re*) vs. mean COT. (b) Scatter plot of *Re* difference (color) vs. transect length and COT using cloud element means.

Sub-pixel heterogeneity and c~~C~~lear sky contamination

660   It has been pointed out by several studies that the bi-spectral *Re* retrieval has a sensitivity to instrument resolution due to a) the nonlinear relationship between VNIR and SWIR reflectances and the COT and *Re* and b) the presence of variability in cloudy reflectances at all scales (e.g., Marshak et al. 2006; Zhang et al. 2012; Zhang et al. 2016; Werner et al. 2018a). An important example of this effect is clear sky contamination, in which cloudy radiances and clear sky radiances are both present within the field of view (FOV) of the sensor. The presence of this sub-pixel clear

665   sky can cause *Re* overestimates of up to 41% when decreasing instrument resolution from 30 m to 1 km (Werner et al. 2018b). The bias in the bi-spectral retrieval due to clear sky contamination decreases monotonically as instrument resolution increases. This is due to the applicability of an independent column approximation as a model of the variability within the FOV due to the negligible atmospheric and surface scattering contributions over ocean surfaces to VNIR and SWIR radiance. Other reflectance variations within cloudy portions of an instrument FOV also cause a

670   sensitivity of the bi-spectral retrieval to instrument resolution, though this is typically smaller, being 1 - 3 μm (Zhang

et al. 2016; Werner et al. 2018a). In this case, increasing instrument resolution does not necessarily cause a monotonic reduction in retrieval bias (e.g., Davis et al. 1997; Zhang et al. 2012). That is because the relationship between the heterogeneity of the optical and microphysical properties (e.g., Re) within the cloud and the radiance field is governed by 3-D radiative transfer, not an independent column approximation. Note that polarimetric retrievals are only weakly sensitive to instrument resolution as they are largely unaffected by clear sky contamination (e.g., Miller et al. 2018; Shang et al. 2015). Based on these considerations, we assess the sensitivity of our bias estimate in the bi-spectral Re due to the relative coarse resolution of RSP by investigating the impact of clear sky contamination using the higher resolution HSRL-2 lidar. We may then attribute the remaining bias in Re to the expression of cloud heterogeneity and 3-D radiative transfer, whether this occurs at resolved or unresolved (i.e., sub-pixel to HSRL-2) scales.

Another potential factor that could lead to considerable Re bias, as have been pointed out by several studies, is sub-pixel reflectance variations (e.g., Marshak et al. 2006; Zhang et al. 2012; Zhang et al. 2016; Werner et al. 2018). To give one such example, when partially cloudy regions are mixed with clear sky regions, low surface albedo (e.g., over ocean) would contribute to smaller nadir reflectance in the SWIR channel and lead to overestimated Re retrievals compared to the true Re (e.g., Marshak et al. 2006). Attempts have been made to understand the magnitude of clear sky contamination on Re retrievals. For example, Werner et al. (2018) used hi-resolution (30 m) ASTER data to improve the bi-spectral Re retrievals for partly cloudy observations and showed the overestimates in retrieved Re at MODIS pixel scales can exceed 41% due to clear sky contamination. For polarimetric Re retrievals, since it is sensitive to the angular shape of the supernumerary bow from polarized reflectances, the presence of clear sky does not strongly distort the shape of the supernumerary bows from cloud scattering, so polarimetric Re are not significantly affected by clear sky contamination or sub-pixel heterogeneity. (e.g., Miller et al. 2018; Shang et al. 2015).

For CAMP²Ex, given the statistics of the sampled clouds (Fig. 2), the abundance of small (transect length) and optically thin clouds (Fig. 8) led to our investigation of clear sky contamination to the observed Re differences between RSP bi-spectral and polarimetric retrievals. The RSP instrument's 14 mrad IFOV converts to a roughly ~120 m horizontal footprint for the cloud retrievals. We used HSRL-2 2Hz data (~75 m horizontal resolution) to derive the cloud fraction (CF) for each RSP cloud element in an attempt to identify if RSP identified cloud elements could contain some unresolved clear sky. The higher resolution and greater sensitivity of the HSRL-2 relative to RSP plays out in Figure 2(d) and (e) cloud and clear length statistics, with the largest differences occurring for lengths < 200 m. The good agreement between the two instruments for in cloud lengths > 200 m and for CTH (Fig. 2(c)) indicates similar sensitivity to clouds larger than the RSP footprint. Hence, using HSRL-2 CTH retrievals to derive a cloud fraction for RSP identified cloud elements should provide a relevant sub-pixel cloud fraction for the RSP retrievals. Still, this would be a minimum estimate of clear sky contamination in RSP cloud elements as the lidar itself may also contain unresolved clear sky. For RSP cloud elements that have HSRL-2 CTH retrievals, the HSRL-2 cloud fraction for a RSP cloud element is defined as the number of valid HSRL-2 CTH retrievals divided by the total number of HSRL-2 CTH retrievals within the RSP cloud element. We examined the CDF of RSP cloud elements against HSRL-2 CF and found the following: For clouds with transect lengths under 600m, at least 49% of cloud elements have CF <0.95; for all cloud transect lengths, at least 46% of cloud elements have CF < 0.95. This reveals that at least about half of the cloud elements have some degree of clear sky contamination (CF<0.95). We are interested in how the

amount of clear sky contamination can impact the observed differences between bi-spectral and polarimetric *Re* retrievals.

710   To further investigate how *Re* differences depend on HSRL-2 CF, the cloud elements are separated into partly cloudy (CF < 0.5), mostly cloudy (0.5 < CF < 0.95) and overcast (CF > 0.95), and further divided into small transect length (< 2 km) and large transect length (> 2 km) populations. Figure 9 shows the PDFs of the three CF groups segregated by the two cloud size groups. For transect lengths smaller than 2 km (solid lines in Fig. 9), the three CF groups have similar distributions, with median values of *Re* differences of 8.9 μm, 7.3 μm and 8.1 μm for partly

715   cloudy, mostly cloudy and overcast, respectively. For transect lengths greater than 2 km (dash lines in Fig. 9), there are no samples for CF < 0.5 (hence no red dashed histogram) and the median values of the *Re* differences are 5.3 μm and 5.7 μm for mostly cloudy and overcast groups, respectively. Thus, sub-pixel clear-sky contamination (derived from HSRL-2 2Hz) appears to account for < ~1 μm in the *Re* differences, with transect lengths playing a larger role since the median value of the small-size group being 2.4 μm larger than the large-size group in the *Re* differences. To

720   summarize, from the RSP cloud element analysis, the large *Re* difference between the two techniques is found to be more related to optical depth and transect length than sub-pixel clear-sky contamination for the RSP warm cloud samples observed during CAMP^{2}Ex.
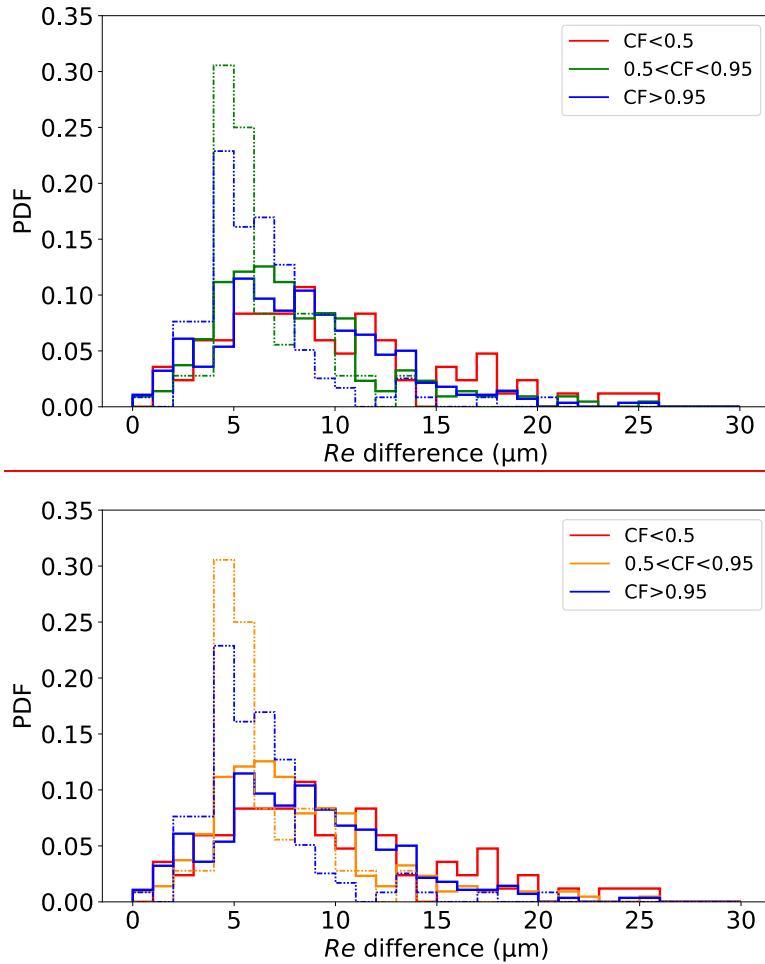
Figure 9. PDF of *Re* difference stratified by CF < 0.5 (11% of all cloud elements), 0.5 < CF < 0.95 (34% of all cloud elements) and CF > 0.95 (54% of all cloud elements) for cloud elements with transect lengths less than 2 km (79% of all cloud elements, solid) and greater than 2 km (21% of all cloud elements, dash). There are no samples for CF<0.5 for transect lengths greater than 2 km.

Cloud top bumpiness and solar zenith angle

In our cloud element analysis, we defined cloud top bumpiness as the standard deviation of CTH for each cloud element, with the idea that it can capture the variation in cloud top structure for each cloud element. As pointed out by Loeb et al. (1998), not accounting for sub-pixel variations in CTH in the plane parallel assumption leads to large biases in retrieved COT, particularly at large SZA. More recent studies have shown that polarimetric *Re* retrievals are less susceptible to cloud top bumpiness (e.g., Cornet et al. 2018). In our analysis, we used HSRL-2 2 Hz CTH to derive cloud top bumpiness, where the 2 Hz HSRL-2 data converts to a roughly ~75 m horizontal resolution. To avoid clear sky contamination, we separated overcast cloud elements from partly and mostly cloudy cloud elements as above. When the differences in RSP bi-spectral and polarimetric *Re* retrievals are organized as a function of HSRL-2 cloud top bumpiness, no apparent dependence was observed in the overcast cases (not shown). This might be due to the fact that the possible effects of cloud top bumpiness on *Re* differences is masked by the effect of cloud size, since the clouds with the smallest transect length also have the smallest CTH standard deviation.

Past literature that examined the dependence of *Re* bias on SZA through simulations and observation studies typically show that SZA contributions to *Re* variations of ~1 to 2 μm. (e.g., Zhang et al. 2012; Grosvenor and Wood 2014; Horváth et al. 2014; Ahn et al. 2018). We also examined the impact of Solar Zenith Angle (SZA) on the RSP *Re* retrievals with our cloud element analysis, noting that the RSP retrievals rarely had cloud samples under low sun conditions (SZA <60°), with most samples taken with SZA between 20° and 45°. Similar to the findings in Ahn et al. (2018) and Grosvenor and Wood (2014), the cloud element *Re* difference does not seem to be sensitive to SZA, possibly due to the small range of SZA in which RSP retrievals were collected, along with the complexity of the co-variability between different cloud variables and 3-D pathways (e.g., shadowing vs illumination, leakage vs channeling).

4.2.2 Drizzle

In our analysis, we used the maximum APR-3 W-band reflectivity over a cloud element as a proxy for in-cloud drizzle for that cloud element. We examined the sensitivity of the differences between RSP bi-spectral and polarimetric retrievals of *Re* to the APR-3 reflectivity. To determine the effect of the single mode droplet size distribution assumption in the bi-spectral technique, we further restricted the maximum of APR-3 W-band reflectivity to be ~100 m from the cloud top of each cloud element. We also experimented using a column maximum W-band reflectivity and the results are very similar with using ~100 m from the cloud top.

Figure 10 shows the *Re* differences between RSP polarimetric and bi-spectral retrievals of all the cloud elements binned by W-band reflectivity in 5 dBZ intervals. Past studies have shown that we can be certain that W-band reflectivities < -20 dBZ contain no drizzle, light drizzle between ~ -15 dBZ to -7.5 dBZ, and rain for > 0 dBZ (e.g., Dzambo et al. 2019; Wang and Geerts 2003; Sauvageot and Omar, 1987). The largest mean *Re* difference of 9.2 μm (with a standard deviation of 5.6 μm) was observed for Z < -20 dBZ, and the smallest mean *Re* difference of 3.1 μm

(with a standard deviation of 1.7 μm) was observed for 0 < Z < 5 dBZ. Figure 10~~2~~ also reveals a large range of *Re* difference values (of up to 25 μm) for bins with Z < -15 dBZ, whereas a trend of decreasing range and maximum *Re* difference is observed for bins with Z > -15 dBZ. While no clear sensitivity of *Re* difference on W-band Reflectivity is suggested, Fig. 10 indicates that observed large *Re* differences especially for bins with Z < - 15 dBZ could not be explained by drizzle. Therefore, we conclude that it is not likely that the difference in the bi-spectral and polarimetric *Re* can be explained by drizzle alone. This aligns with findings from Zhang et al. (2012) and Ahn et al. (2018).
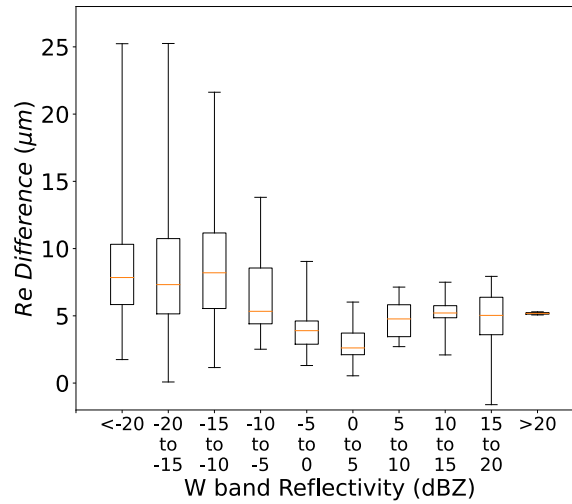
Figure 10. RSP cloud element *Re* difference using all RSP cloud elements across all RFs, binned by APR-3 W-band Max reflectivity intervals of 5 dBZ. Orange line indicates median for each bin, the box ends indicate interquartile, and the end of whiskers indicate maximum and minimum values for each bin.

4.3 Consistency of *Re* retrieval representativeness from CAMP²Ex

Lastly, the consistency between *Re* retrievals across all techniques is examined for the CAMP²Ex region. In doing so, we seek to gauge the representativeness of Terra-MODIS *Re* retrievals by comparing to RSP (airborne remote sensing) and in situ measurements sampled across all RFs. Level 2 liquid *Re* retrievals from Terra-MODIS within the CAMP²Ex region (Fig. 1) from all 19 P-3 Research Flight days were included to derive a *Re* distribution. All valid *Re* retrievals from RSP and MODIS *Re* are included after removing cirrus and ice clouds indicated by SPN-S and MODIS phase flag. For in situ measurements, again to avoid sampling differences with passive remote sensing (i.e., in situ sampling through deep convective clouds which was not sampled by RSP), in situ samples ~~were removed~~ with 11μm Brightness Temperature < 273K were removed as indicated from AHI. Figure 11 shows the *Re* distributions from MODIS and RSP and in situ measurements. Given the difference in resolution and spectral channel, RSP-polarimetric and bias-adjusted MODIS *Re* agrees within 1 μm as indicated by the median and mean values in Table 5. The two also have very similar variability as indicated by the standard deviations. The RSP bi-spectral and the original MODIS *Re* also have similar *Re* statistics that agree within ~2 μm of each other, but both are also 5 - 7 μm larger than RSP-Polarimetric and bias-adjusted MODIS Re with larger standard deviations. In situ derived *Re* from the P-3 and Learjet indicates a median of 11.0 μm and 12.4 μm, which agrees to RSP-polarimetric and bias-adjusted MODIS *Re* within ~ 2 μm. Longer tails in the distributions of *Re* from in situ measurements are not limited by the 30

μm cut-off in the bi-spectral retrievals LUT. Also, as noted in Sect. 3, they are associated with the penetration of deeper clouds at altitudes different to the CTH level observed by the remote sensing, with the clouds tending to contain rain. This long tail contributes to the much larger mean and standard deviation relative to the remote sensing retrievals. Overall, *Re* observations from the RSP polarimetric, the bias-adjusted MODIS *Re*, the Learjet in situ, and the P-3 in situ indicated similar median *Re* values of ~10 - 12 μm, while MODIS *Re* and RSP bi-spectral *Re* show overestimates of ~ 5 - 7 μm compared to the other techniques. This is also consistent with the results from the individual case studies in Sect. 3.3.
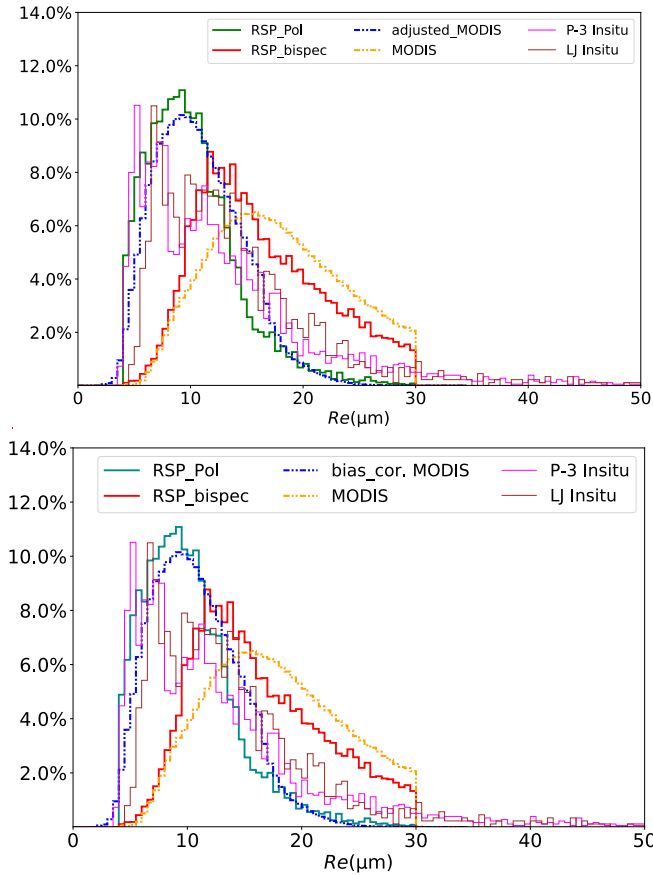
Figure 11. *Re* distributions from L2 RSP polarimetric *Re*, L2 RSP bi-spectral *Re*, L2 MODIS *Re*, L2 MODIS bias-adjusted *Re*, 1 Hz P-3 in situ derived *Re*, 1 Hz Learjet in situ derived *Re* using all valid retrievals of warm oceanic clouds within the domain indicated in Fig. 1.

Table 5. *Re* statistics averaged over all research flight segments for warm clouds.

	Median (μm)	Mode (μm)	Mean ± Standard deviation (μm)
RSP Polarimetric *Re*	9.6	9.0	10.2 ± 4.0
MODIS Adjusted *Re*	10.4	9.0	10.8 ± 3.8
P-3 in situ *Re*	11.0	5.0	13.6 ± 11.3
Learjet in situ *Re*	12.4	6.5	15.2 ± 12.1
RSP bi-spectral *Re*	15.1	11.5	16.2 ± 5.5
MODIS *Re*	17.2	15.5	17.7 ± 5.7

To test the similarity of the different *Re* distributions shown in Fig. 11, a Kolmogorov-Smirnov (K-S) test was applied to all 6 *Re* distributions, with the results listed in Table 6. When the other five *Re* distributions are compared with the RSP polarimetric *Re* distribution, both the RSP bi-spectral *Re* and MODIS *Re* distributions have p-values < 0.05, which indicates that these two *Re* distributions do not belong to the same distribution as the RSP polarimetric *Re* distribution. Bias-adjusted MODIS, P-3 in situ and Learjet in situ *Re* distributions, however, have p-values > 0.05, and therefore we cannot reject the null hypothesis that these three *Re* distributions belong to the same distribution as the RSP polarimetric *Re* distribution. Among the three distributions, bias-adjusted MODIS *Re* has the smallest K-S value and the highest p-value, which indicates it is overall the closest fit to RSP polarimetric *Re* distribution. The K-S results are consistent with the difference in the *Re* median values from Table 5, i.e., RSP polarimetric, bias-adjusted *Re*, P-3 in situ and Learjet in situ have closer median *Re* values that are within 1 to 2 μm, while RSP bi-spectral *Re* and MODIS *Re* median values are 5 to 7 μm larger than that from the RSP-polarimetric *Re*. We also examined the similarity for CTH distributions retrieved from RSP and MODIS, and obtained a K-S statistic of 0.32 with a p-value of 0.31. Therefore, we cannot reject the null hypothesis that the two CTH distributions belong to the same distribution. Similarly, when Learjet and P-3 sampling altitude distributions averaged across all flight segments are compared, the two in situ sampling distributions have a K-S statistic of 0.16 and a p-value of 0.98. Thus, we conclude that the two in situ techniques sampled similar cloud fields during CAMP²Ex, and RSP and MODIS cloud samples also came from similar cloud fields during CAMP²Ex.

While we have been using the MODIS *Re* product derived from its 2.1 μm channel, we also examined the MODIS *Re* derived from its 3.7 μm channel. For MODIS *Re* derived from its 3.7 μm channel, the median, mode, and mean ± standard deviation are, 14.3, 12.5, and 15 ± 4.8 μm, respectively, for warm clouds over all research flights. Comparing these values to those in Table 5, we see that the MODIS 3.7 μm retrievals are ~ 2 to 3 μm smaller than MODIS 2.1 μm retrievals, which is thought to be due a combination of less impact from 3-D effects and differences in the vertical weighting of the two channels (e.g., Zhang and Platnick 2011). The MODIS 3.7 μm retrievals are still larger than the RSP polarimetric retrievals by ~3 to 5 μm.

Table 6. Kolmogorov-Smirnov test for similarity statistics, using RSP Polarimetric *Re* distribution as the reference.

Compared to RSP Polarimetric *Re* dist.	K-S statistics	p-value
RSP Bi-spectral	0.31	0.008
MODIS	0.34	0.002
Bias-adjusted MODIS	0.10	0.92
P-3 in situ	0.20	0.09
Learjet in situ	0.19	0.112

5 Conclusions

This paper presents the first field evaluation of satellite bi-spectral *Re* retrievals in tropical cumulus cloud fields. The evaluation consists of comparison between airborne RSP bi-spectral and polarimetric retrievals of *Re*, and cross-comparison between airborne remote sensing, in situ and satellite retrieved *Re* collected during the CAMP²Ex field campaign. Unlike previous studies that used field data for evaluating satellite bi-spectral retrievals of stratocumulus

cloud fields, validation in cumulus cloud fields presents a greater challenge since they are less persistent, with fast changing cloud morphologies and complex cloud structures. Here, we take a full advantage of RSP's capability to provide both collocated bi-spectral and polarimetric *Re* retrievals; thus there is no sampling difference in comparing the two retrieval techniques. We show that the RSP bi-spectral *Re* retrieved in CAMP²Ex cloud fields is on average overestimated by 6.0 µm compared to the RSP polarimetric *Re* for the 1.2 Hz samples across the entire mission. RSP polarimetric *Re* also indicates much less variability and a clear increase with CTH compared to RSP bi-spectral *Re*.

MODIS *Re* retrievals, which uses a bi-spectral approach, isare in good agreement with RSP bi-spectral *Re* (median *Re* difference within 2.1 µm from Table 5). The bias-adjusted MODIS *Re*, based on the Fu et al. (2019) bias-correction factors, shows tight agreement with the RSP polarimetric *Re* (median *Re* difference within 0.8 µm from Table 5). The bias-adjusted MODIS *Re* and the RSP polarimetric *Re* both show increasing profiles with CTH, and less variability compared to the original MODIS *Re*. The in situ measured *Re* values are in good agreement (median *Re* difference within 2.8 µm from Table 5) with the RSP-polarimetric and bias-adjusted MODIS *Re* values. Further restricting altitudes to CTH < 2 km for shallow convection yields better agreement (median *Re* within 1.7 µm) between them. Thus, these three independent techniques are in very good agreement with each other and are ~5.5 - 7.6 µm smaller than the median *Re* values from the bi-spectral *Re* from RSP and MODIS. These agreements were found to be consistent between mission averaged statistics (Table 5) and case by case comparison (Table 3). For deeper clouds containing in situ measured precipitation, in situ measures of *Re* can at times be much larger than all of the remotely sensed *Re* values.

By taking advantage of collocated RSP, APR-3 and HSRL-2 on the P-3, we further examined the differences in RSP bi-spectral and polarimetric *Re* and how they relate to cloud macrophysics (cloud transect length, cloud top bumpiness, sub-pixel cloud fraction), COT, SZA and drizzle. We found that *Re* differences (bi-spectral – polarimetric) of up to 25 µm (median 11 µm) is associated with small COT (COT < 5). As COT increases from 5 to 15, the *Re* difference maximum decreases to ~ 5 µm (median ~3 µm). For COT greater than 15, there is no clear dependence of *Re* difference on COT. Similarly, *Re* differences of up to 26 µm (median ~8 µm) are associated with the smallest cloud transect lengths (< 0.5 km). For cloud transect lengths greater than 5 km, *Re* differences drop to 10 µm (median ~5 µm). RSP cloud retrievals have clear sky contamination, as revealed by higher resolution HSRL-2 data. Clear sky contamination is shown to have only a minor impact on *Re* differences (< 1µm) relative to fully cloudy pixels. No apparent relationships between *Re* differences and SZA and cloud top bumpiness are observed, noting that the range of SZA sampled during RSP *Re* retrievals was small under moderately high sun condition (SZA = 20° to 45°) and the co-variability of cloud top bumpiness with other cloud variables. 80% of the cloud elements sampled by RSP contained some degree of drizzle within cloud as revealed by APR-3, and a general decreasing trend of *Re* differences is observed for the lowest W-band reflectivities. Separating by non-drizzle and drizzle samples by -15 dBZ reveals that, on average, cloud elements with detectable drizzle have *Re* differences that are ~ 1 µm smaller than cloud elements with no detectable drizzle.

Our analysis in Sect. 3.1 showed that most samples observed by the P-3 remote sensors came from small, optically thin, shallow clouds. The samples exhibit a large difference (~factor of 2) between RSP bi-spectral and polarimetric *Re* retrievals. For non-drizzling shallow clouds, in situ observations compare well against the RSP polarimetric

870   retrievals, and show variability of within ~2 μm. For these non-drizzling shallow clouds, no in situ Re samples are as large as the RSP bi-spectral Re. Therefore, for the shallow clouds observed by RSP during CAMP²Ex, the long-held hypothesis of the presence of drizzle or vertical variations as major contributing factors to Re differences between bi-spectral and polarimetric retrievals could be rejected with near certainty. Also, as revealed by the HSRL-2 derived RSP cloud element cloud fraction, clear sky contamination only has very limited contribution (~1 μm) to the observed

875   RSP Re differences. Thus, for the shallow, non-drizzling clouds, the evidence presented herein is strongly suggestive that the dominant cause for the differences between RSP polarimetric and bi-spectral Re observed during CAMP²Ex is ~~lies within~~due to 3-D radiative ~~pathways~~ transfer and cloud heterogeneity (both resolved and unresolved by RSP) effects that lead to large positive biases in bi-spectral retrievals of Re compared to polarimetric retrievals. For deeper clouds that contain drizzle, true in-cloud vertical variations could still be at play in explaining additional Re differences

880   between bi-spectral and polarimetric techniques.

       For MODIS, there is a substantial number of partly cloudy pixels as revealed by coincident, high-resolution ASTER data. These sub-pixel clouds often lead to failed MODIS retrievals of Re, as discussed in Cho et al. (2015). Comparing the cloud macrophysical properties for CAMP²Ex reported in Sect. 3.1 with those reported for RICO and INDOEX, the CAMP²Ex shallow clouds have more numerous smaller clouds. We speculate that the reason for the

885   maximum failure rate in MODIS cloud microphysical retrievals occurring over the western tropical Pacific, as reported by Cho et al. (2015), may be because of the high frequency of small clouds here relative to anywhere else. Still, as shown in Sect. 4.3, we cannot reject the null hypothesis that the MODIS CTH distributions belong to the same distributions observed by the RSP from P-3. This provides confidence that the conclusions drawn from the RSP polarimetric and bi-spectral Re comparison extend to MODIS as well.

890   This study also provides additional validation of the bias-adjusted MODIS Re values reported in Fu et al. (2019), showing a mission averaged mean ± standard deviation of 10.8 ± 3.8 μm compared to RSP polarimetric Re values of 10.2 ± 4 μm as shown in Table 5. Throughout, we used the upper-bound Re bias adjustment factors of Fu et al. (2019), rather than present both upper- and lower-bound estimates, simply to reduce clutter within many of the figures. However, both were examined. Using the lower-bound bias adjustment factors leads to a mission mean ± standard

895   deviation of 6.7 ± 3.2 μm. The RSP polarimetric Re falls between the upper and lower bounds estimates. Fu et al. (2019) showed that the largest regional Re biases for marine liquid water clouds occur over the tropical western pacific, and our results seem to indicate that this may be because of a higher frequency of smaller clouds here relative to everywhere else. Our validation here, along with in situ validation of MODIS Re from other regions (e.g., Painemal and Zuidema 2011, Ahn et al. 2018), provides additional confidence in the global distribution of bias-adjusted MODIS

900   Re reported in Fu et al. (2019).

       Data availability. CAMP²Ex datasets of RSP, APR-3, HSRL-2, SPN-S, P-3 collocated AHI CLAVR-X data products, SPEC in situ data used in this analysis are available at: https://www-air.larc.nasa.gov/cgi-bin/ArcView/camp2ex. CAMP²Ex P-3 and Learjet forward videos can be access at: https://asp-archive.arc.nasa.gov/CAMP2EX/N426NA/video/ and https://www-air.larc.nasa.gov/cgi-

905   bin/ArcView/camp2ex?LEARJET=1. MODIS Collection 6.1 cloud products (dx.doi.org/10.5067/MODIS/MOD06_L2.061), MODIS Level 1B Calibrated radiances at 250m

(dx.doi.org/10.5067/MODIS/MOD02QKM.061) and 500m (dx.doi.org/10.5067/MODIS/MOD02HKM.061) were obtained through the level 1 and Atmosphere Archive and Distribution System of NASA Goddard Space Flight Center (https://ladsweb.modaps.eosdis.nasa.gov). The MODIS bias-adjusted *Re* correction factors can be found at: https://doi.org/10.17632/j4r72zxc6g.2. AHI standard cloud products are available at: https://www.eorc.jaxa.jp/ptree/index.html. The 10-minute AHI 1km reflectances imagery can be accessed from the CAMP²Ex Worldview interface (http://geoworldview.ssec.wisc.edu).

Author contribution. DF performed the analysis and drafted the manuscript. The methodology was developed by DF, LDG. LDG, JL, BvD, YH, GMM, RMR, SWN helped with the writing and editing of the manuscript at various stages. RSP retrievals used in this study was supported by BC, MA, BvD. PL, SW collected, processed, and curated in-situ measurements used in this study. APR-3 data was supported by TS, OOS collected, processed, and curated APR-3 data. CH and AJS collected, processed, and curated HSRL-2 dataset. SS provided the SPN-S dataset and YH derived SPN-S transmittance. All authors contributed to the editing of the manuscript.

Acknowledgements. The authors would like to acknowledge NASA grant numbers 80NSSC18K0144, 80NSSC18K0150, 80NSSC18K0146, and 80NSSC21K1449 and their program manager, Dr. Hal Maring. We thank all the members of the CAMP²Ex team for their hard work in collecting the datasets analyzed herein. We also thank Dr. Guangyu Zhao for his help in providing reprojected overlays of ASTER and MODIS data. We are grateful for the discussion with Graeme Stephens and for comments from two anonymous reviewers.

Competing interests. The authors declare that they have no conflict of interest.

References

Abrams, M.: The Advanced Spaceborne Thermal Emission and Reflection Radiometer (ASTER): Data products for the high spatial resolution imager on NASA's Terra platform, Int. J. Remote Sens., 21:5, 847-859, https://doi.org/10.1080/014311600210326, 2000.

Ahn, E., Huang, Y., Siems, S. T., and Manton, M. J.: A comparison of cloud microphysical properties derived from MODIS and CALIPSO with measurements over the wintertime southern ocean, J. Geophys. Res. Atmos., 123, 11,120–11,140, https://doi.org/10.1029/2018JD028535, 2018.

Alexandrov, M.D., Cairns, B., Emde, C., Ackerman, A. S., van Diedenhoven, B.: Accuracy assessments of cloud droplet size retrievals from polarized reflectance measurements by the research scanning polarimeter, Remote Sens. Environ., 125,92-111, https://doi.org/10.1016/j.rse.2012.07.012, 2012.

Alexandrov, M.D., Cairns, B., Sinclair, K., Wasilewski, A.P., Ziemba, L., Crosbie, E., Moore, R., Hair, J., Scarino, A. J., Hu, Y., Stamnes, S., Shook, M.A., and Chen, G.: Retrievals of cloud droplet size from the research scanning polarimeter data: Validation using in situ measurements. Remote Sens. Environ., 210, 76-95, https://doi.org/10.1016/j.rse.2018.03.005, 2018.

Alexandrov, M.D., Cairns, B., Wasilewski, A.P., Ackerman, A. S., McGille, M. J., Yorks, J. E., Hlavka, D. L., Platnick, S. E., Arnold, G. T., van Diedenhoven, B., Chowdhary, J., Ottaviani, M., Knobelspiesse, K. D.: Liquid

water cloud properties during the Polarimeter Definition Experiment (PODEX), Remote Sens. Environ., 169, 20–36, https://doi.org/10.1016/j.rse.2015.07.029, 2015.

Arabas, S., Pawlowska, H., and Grabowski, W. W.: Effective radius and droplet spectral width from in-situ aircraft observations in trade-wind cumui during RICO. Geophys. Res. Lett., 36, L11803, https://doi.org/10.1029/2009GL038257, 2009.

Badosa, J., Wood, J., Blanc, P., Long, C. N., Vuilleumier, L., Demengel, D., and Haeffelin, M.: Solar irradiances measured using SPN1 radiometers: uncertainties and clues for development, Atmos. Meas. Tech., 7, 4267–4283, https://doi.org/10.5194/amt-7-4267-2014, 2014.

Ban-Weiss, G. A., Jin, L., Bauer, S. E., Bennartz, R., Liu, X., Zhang, K., Ming, Y., Guo, H., and Jiang, J.: Evaluating clouds, aerosols, and their interactions in three global climate models using satellite simulators and observations, J. Geophys. Res. Atmos., 119, 10,876–10,901, https://doi.org/10.1002/2014JD021722, 2014.

Bannehr, L., and Glover, V.: Preprocessing of airborne pyranometer data, No. NCAR/TN-364+STR, University Corporation for Atmospheric Research, https://doi.org/10.5065/D6MK69T4, 1991.

Barron, N. R., Shawn D. Ryan, S. D., and Heus, T.: Reconciling chord length distributions and area distributions for fields of fractal cumulus clouds, Atmosphere, 11, 824, https://doi.org/10.3390/atmos11080824, 2020.

Bessho, K., Date, K., Hayashi, M., Ikeda, A., Imai, T., Inoue, H., Kumagai, Y., Miyakawa, T., Murata, H., Ohno, T., Okuyama, A., Oyama, R., Sasaki, Y., Shimazu, Y., Shimoji, K., Sumida, Y., Suzuki, M., Taniguchi, H., Tsuchiyama, H., Uesawa, D., Yokota, H., and Yoshida, R.: An introduction to Himawari-8/9—Japan's new-generation geostationary meteorological satellites, J. Meteor. Soc. Japan, 94, 151–183, https://doi.org/10.2151/jmsj.2016-009, 2016.

Brenguier, J., Bourrianne, T., Coelho, A. A., Isbert, J., Peytavi, R., Trevarin, D., and Weschler, P.: Improvements of droplet size distribution measurements with the Fast-FSSP (Forward Scattering Spectrometer Probe), J. Atmos. Ocean. Tech., 15(5), 1077-1090, https://doi.org/10.1175/1520-0426(1998)015<1077:IODSDM>2.0.CO;2, 1998.

Bréon, F.-M., and Doutriaux-Boucher, M.: A comparison of cloud droplet radii measured from space, IEEE Trans. Geosci. Remote Sens., 43, 1796–1805, https://doi.org/10.1109/tgrs.2005.852838, 2005.

Burton, S. P., Hostetler, C. A., Cook, A. L., Hair, J. W., Seaman, S. T., Scola, S., Harper, D. B., Smith, J. A., Fenn, M. A., Ferrare, R. A. and Saide, P.E.: Calibration of a high spectral resolution lidar using a Michelson interferometer, with data examples from ORACLES. Appl. Opt., 57(21), 6061-6075, https://doi.org/10.1364/AO.57.006061, 2018.

Cairns, B., Russell, E. E., and Travis, L. D.: Research Scanning Polarimeter: calibration and ground-based measurements, Proc. SPIE 3754, Polarization: Measurement, Analysis, and Remote Sensing II, https://doi.org/10.1117/12.366329, 1999.

Cao, C., De Luccia, F. J., Xiong, X., Wolfe, R., and Weng, F.: Early on-orbit performance of the Visible Infrared Imaging Radiometer Suite onboard the Suomi National Polar-orbiting Partnership (S-NPP) satellite. IEEE Trans. Geosci. Remote Sens., 52, 1142-1156, https://doi.org/10.1109/TGRS.2013.2247768, 2014.

Chang, F. L., and Li, Z. Q.: A new method for detection of cirrus overlapping water clouds and determination of their optical properties, J. Atmos. Sci., 62(11), 3993–4009, 2005.

Cho, H.-M., Zhang, Z., Meyer, K., Lebsock, M., Platnick, S., Ackerman, A. S., Di Girolamo, L., Labonnote, L., Cornet, C., Riedi, J., and Holz, R. E.: Frequency and causes of failed MODIS cloud property retrievals for liquid phase clouds over global oceans, J. Geophys. Res. Atmos., 120, 4132–4154, https://doi.org/10.1002/2015JD023161, 2015.

Cornet, C., C.-Labonnote, L., Waquet, F., Szczap, F., Deaconu, L., Parol, F., Vanbauce, C., Thieuleux, F., and Riédi, J.: Cloud heterogeneity on cloud and aerosol above cloud properties retrieved from simulated total and polarized reflectances, Atmos. Meas. Tech., 11, 3627–3643, https://doi.org/10.5194/amt-11-3627-2018, 2018.

Curry, J. A., Hobbs, P. V., King, M. D., Randall, D. A., Minnis, P., Isaac, G. A., Pinto, J. O., Uttal, T., Bucholtz, A., Cripe, D. G., Gerber, H., Fairall, C. W., Garrett, T. J., Hudson, J., Intrieri, J. M., Jakob, C., Jensen, T., Lawson, P., Marcotte, D., Nguyen, L., Pilewskie, P., Rangno, A., Rogers, D. C., Strawbridge, K. B., Valero, F. P. J., Williams, A. G., and Wylie, D.: FIRE arctic clouds experiment, Bull. Ameri. Meteor. Soc., 81(1), 5– 29. https://doi.org/10.1175/1520-0477(2000)081<0005:face>2.3.co;2, 2000.

Davis, A., Marshak, A., Cahalan, R., and Wiscombe, W.: The Landsat scale break in stratocumulus as a three-dimensional radiative transfer effect: Implications for cloud remote sensing, J. Atmos. Sci., 54(2), 241-260, https://doi.org/10.1175/1520-0469(1997)054<0241:TLSBIS>2.0.CO;2, 1997.

Di Girolamo, Liang, L., L., and Platnick, S.: A global view of one-dimensional solar radiative transfer through oceanic water clouds, Geophys. Res. Lett., 37, L18809, https://doi.org/10.1029/2010GL044094, 2010.

Di Girolamo, L., Holz, R., Reid, J., Tanelli, S., van den Heever, S., Narsma, G., and Simpas, J.: Cloud and aerosol monsoonal processes-Philippines experiment (CAMP^{2}Ex), https://espo.nasa.gov/CAMP2Ex_White_Paper, last access: 24, Dec., 2021, 2015.

Diner, D. J., Beckert, J. C., Reilly, T. H., Bruegge, C. J., Conel, J. E., Kahn, R.A., Martonchik, J.V., Ackerman, T. P., Davies, R., Gerstl, S.A.W., Gordon, H.R., Muller, J-P., Myneni, R., Sellers, R.J., Pinty, B., and Verstraete, M.M.,: Multi-angle Imaging SpectroRadiometer (MISR) instrument description and experiment overview. IEEE Trans. Geosci. Remote Sens., 36(4), 1072–1087, https://doi.org/10.1109/36.700992, 1998.

Durden, S. L., Tanelli, S., and Sy, O. O.: Comparison of GPM DPR and airborne radar observations in OLYMPEX, IEEE Geosci. Remote Sens. Lett., 17, 10, pp. 1707-1711, https://doi.org/10.1109/LGRS.2019.2952287, 2020.

Dzambo, A. M., L'Ecuyer, T., Sy, O. O., and Tanelli, S.: The observed structure and precipitation characteristics of southeast Atlantic stratocumulus from airborne radar during ORACLES 2016–17, *J. Appl. Meteor. Climatol.*, *58*(10), 2197-2215, https://doi.org/10.1175/JAMC-D-19-0032.1, 2019.

Fu, D., Di Girolamo, L., Liang, L., and Zhao, G.: Regional biases in MODIS marine liquid water cloud drop effective radius deduced through fusion with MISR. J. Geophys. Res. Atmos., 124, 13182–13196, https://doi.org/10.1029/2019JD031063, 2019.

Gupta, S., McFarquhar, G. M., O'Brien, J. R., Poellot, M. R., Delene, D. J., Miller, R. M., and Small Griswold, J. D.: Precipitation Susceptibility of Marine Stratocumulus with Variable Above and Below-Cloud Aerosol Concentrations over the Southeast Atlantic, Atmos. Chem. Phys., 22, 2769-2793, https://doi.org/10.5194/acp-22-2769-2022, 2022.

Gerber, H., Frick, G., Jensen, J., and Hudson, J.: Entrainment, mixing, and microphysics in trade-wind cumulus, J. Meteorol. Soc. Jpn., 86, 87–106. https://doi.org/10.2151/jmsj.86A.87, 2008.

Grosvenor, D. P., and Wood, R.: The effect of solar zenith angle on MODIS cloud optical and microphysical retrievals within marine liquid water clouds. Atmos. Chem. Phys., 14, 7291–7321, https://doi.org/10.5194/acp-14-7291-2014, 2014.

Gryspeerdt, E., Goren, T., Sourdeval, O., Quaas, J., Mülmenstädt, J., Dipu, S., Unglaub, C., Gettelman, A., and Christensen, M.: Constraining the aerosol influence on cloud liquid water path, Atmos. Chem. Phys., 19, 5331–5347, https://doi.org/10.5194/acp-19-5331-2019, 2019.

Hair J, Hostetler C, Cook A, Harper D, Ferrare R, Mack T, Welch W, Izquierdo L, and Hovis F.: Airborne high spectral resolution lidar for profiling aerosol optical properties, Appl. Opt., 47, 6734-6752, https://doi.org/10.1364/AO.47.006734, 2008.

Horváth, Á., Chellappan, S., and Deneke, H.: View angle dependence of MODIS liquid water path retrievals in warm oceanic clouds. J. Geophys. Res., 119, 8304–8328, https://doi.org/10.1002/2013JD021355, 2014.

IPCC, Climate change 2013: The physical science basis. Contribution of Working Group I to the Fifth Assessment Report of the Intergovernmental Panel on Climate Change [Stocker, T.F., D. Qin, G.-K. Plattner, M. Tignor, S.K. Allen, J. Boschung, A. Nauels, Y. Xia, V. Bex and P.M. Midgley (eds.)]. Cambridge University Press, Cambridge, United Kingdom and New York, NY, USA, 1535 pp. 2013.

Khain, P., Heiblum, R., Blahak, U., Levi, Y., Muskatel, H., Vadislavsky, E., Altaratz, O., Koren, I., Dagan, G., Shpund, J., & Khain, A.: Parameterization of vertical profiles of governing microphysical parameters of shallow cumulus cloud ensembles using LES with bin microphysics, J Atmos. Sci., 76(2), 533-560, https://doi.org/10.1175/JAS-D-18-0046.1, 2019.

Knobelspiesse, K., Tan, Q., Bruegge, C., Cairns, B., Chowdhary, J., van Diedenhoven, B., Diner, D., Ferrare, R., van Harten, G., Jovanovic, V., Ottaviani, M., Redemann, J., Seidel, F., and Sinclair, K.: Intercomparison of airborne multi-angle polarimeter observations from the Polarimeter Definition Experiment, Appl. Opt., 58(3), 650–669, https://doi.org/10.1364/AO.58.000650, 2019.

Lawson, R. P., Stewart, R. E., Strapp, J. W., and Isaac, G. A.: Airborne measurements of the origin and growth of very large snowflakes, Geophys. Res. Lett., 20, 53–56, https://doi.org/10.1029/92GL02917, 1993.

Lawson, R. P., O'Connor, D., Zmarzly, P., Weaver, K., Baker, B., Mo, Q. and Jonsson, H.: The 2D-S (Stereo) probe: Design and preliminary tests of a new airborne, high-speed, high-resolution particle imaging probe, J. Atmos. Oceanic Technol., 23, 1462–1477, https://doi.org/10.1175/JTECH1927.1, 2006.

Lebsock, M. D., and L'Ecuyer T. S.: The retrieval of warm rain from CloudSat, J. Geophys. Res.,116, D20209, https://doi.org/10.1029/2011JD016076, 2011.

Lelieveld J, Crutzen P. J., Ramanathan, V., Andreae, M. O., Brenninkmeijer, C. A. M., Campos, T., Cass, G. R., Dickerson, R. R., Fischer, H., de Gouw, J. A., Hansel, A., Jefferson, A., Kley, D., de Laat, A.T.J., Lal, S., Lawrence, M.G., Lobert J. M., Mayol-Bracero, O. L., Mitra, A. P., Novakov, T., Oltmans, S. J., Prather, K. A., Reiner, T., Rodhe, H., Scheeren, H. A., Sikka, D., and Williams, J.: The indian ocean experiment: Widespread

1050   air pollution from South and Southeast Asia, Science, 291, 1031– 1036, https://doi.org/10.1126/science.1057103, 2001.

Liang, L., and Di Girolamo, L.: A global analysis on the view-angle dependence of plane-parallel oceanic liquid water cloud optical thickness using data synergy from MISR and MODIS, J. Geophys. Res. Atmos., 118, https://doi.org/10.1029/2012JD018201, 2013.

1055   Liang, L., Di Girolamo, L., and Sun, W.: Bias in MODIS cloud drop effective radius for oceanic water clouds as deduced from optical thickness variability across scattering angles. J. Geophys. Res. Atmos., 120, 7661–7681, https://doi.org/10.1002/2015JD023256, 2015.

Loeb, N. G., and Davies, R.: Observational evidence of plane parallel model biases: Apparent dependence of cloud optical depth on solar zenith angle. J. Geophys. Res., 101, 1621–1634, https://doi.org/10.1029/95JD03298, 1996.

1060   Loeb, N. G., Várnai, T., and Winker, D. M.: Influence of sub-pixel scale cloud-top structure on reflectances from overcast stratiform cloud layers, J. Atmos. Sci., 55, 2960–2973, https://doi.org/10.1175/1520-0442(1998)011<0215:IOMSCO>2.0.CO;2, 1998.

Marshak, A., Platnick, S., Várnai, T., Wen, G., and Cahalan, R. F.: Impact of three-dimensional radiative effects on satellite retrievals of cloud droplet sizes. J. Geophys. Res., 111, D09207, https://doi.org/10.1029/2005JD006686,
1065   2006.

McBride, P. J., Schmidt, K. S., Pilewskie, P., Walther, A., Heidinger, A. K., Wolfe, D. E., Fairall, C. W., and Lance, S.: CalNex cloud properties retrieved from a ship-based spectrometer and comparisons with satellite and aircraft retrieved cloud properties, J. Geophys. Res. Atmos., 117, 1–10, https://doi.org/10.1029/2012JD017624, 2012.

McFarquhar, G. M., Bretherton, C. S., Marchand, R., Protat, A., DeMott, P. J., Alexander, S. P., Roberts, G. C.,
1070   Twohy, C. H., Toohey, D., Siems, S., Huang, Y., Wood, R., Rauber, R. M., Lasher-Trapp, S., Jensen, J., Stith, J. L., Mace, J., Um, J., Järvinen, E., Schnaiter, M., Gettelman, A., Sanchez, K. J., McCluskey, C. S., Russell, L. M., McCoy, I. L., Atlas, R. L., Bardeen, C. G., Moore, K. A., Hill, T. C. J., Humphries, R. S., Keywood, M. D., Ristovski, Z., Cravigan, L., Schofield, R., Fairall, C., Mallet, M. D., Kreidenweis, S. M., Rainwater, B., D'Alessandro, J., Wang, Y., Wu, W., Saliba, G., Levin, E. J. T., Ding, S., Lang, F., Truong, S. C. H., Wolff, C.,
1075   Haggerty, J., Harvey, M. J., Klekociuk, A. R., & McDonald, A.: Observations of clouds, aerosols, precipitation, and surface radiation over the Southern Ocean: An overview of CAPRICORN, MARCUS, MICRE, and SOCRATES, Bull. Ameri. Meteor. Soc., 102(4), E894-E928., https://doi.org/10.1175/BAMS-D-20-0132.1, 2021.

McFarquhar, G.M., and Heymsfield, A.J.: The definition and significance of an effective radius for ice clouds. J.
1080   Atmos. Sci., 55, 2039-2052, https://doi.org/10.1175/1520-0469(1998)055<2039:TDASOA>2.0.CO;2, 1998.

McFarquhar, G. M., and Heymsfield, A. J.: Parameterizations of INDOEX microphysical measurements and calculations of cloud susceptibility: Applications for climate studies, J. Geophys. Res. Atmos., 106(D22), 28675-28698, https://doi.org/10.1029/2000JD900777, 2001.

McFarquhar, G.M., Platnick, S., Di Girolamo, L., Wang, H., Wind, G., and Zhao, G.: Remotely sensed observations
1085   of aerosol indirect effects in the Indian Ocean. *Geophys. Res. Lett.*, 31, L21105, https://doi.org/10.1029/2004GL020412, 2004.

McFarquhar, G.M., Zhang, G., Poellot, M.R., Kok, G.L., McCoy, R., Tooman, T., and Heymsfield, A.J.: Ice properties of single layer stratocumulus during the Mixed-Phase Arctic Cloud Experiment (MPACE). Part I: Observations. *J. Geophys. Res.*, 112, D24202, doi:10.1029/2007JD008646, 2007.

Menon, S., Del Genio, A. D., Kaufman, Y., Bennartz, R., Koch, D., Loeb, N., and Orlikowski, D.: Analyzing signatures of aerosol-cloud interactions from satellite retrievals and the GISS GCM to constrain the aerosol indirect effect, J. Geophys. Res., 113, D14S22, https://doi.org/10.1029/2007JD009442, 2008.

Miller, D. J., Zhang, Z., Platnick, S., Ackerman, A. S., Werner, F., Cornet, C., and Knobelspiesse, K.: Comparisons of bispectral and polarimetric retrievals of marine boundary layer cloud microphysics: case studies using a LES–satellite retrieval simulator. Atmos. Meas. Tech., 11, 3689–3715, https://doi.org/10.5194/amt-11-3689-2018, 2018.

Miller, D. J., Segal-Rozenhaimer, M., Knobelspiesse, K., Redemann, J., Cairns, B., Alexandrov, M., van Diedenhoven, B., and Wasilewski, A.: Low-level liquid cloud properties during ORACLES retrieved using airborne polarimetric measurements and a neural network algorithm, Atmos. Meas. Tech., 13, 3447–3470, https://doi.org/10.5194/amt-13-3447-2020, 2020.

Nakajima, T., and King, M. D.: Determination of the optical thickness and effective particle radius of clouds from reflected solar radiation measurements. Part I: Theory. J. Atmos. Sci., 47, 1878–1893, https://doi.org/10.1175/1520-0469 (1990) 047<1878:DOTOTA>2.0. C O;2, 1990.

Nakajima, T., King, M. D., Spinhirne, J. D., and Radke, L. F.: Determination of the optical thickness and effective particle radius of clouds from reflected solar radiation measurements. Part II: Marine stratocumulus observations, J. Atmos. Sci., 48, 728–751, https://doi.org/10.1175/1520-0469(1991)048<0728:DOTOTA>2.0.CO;2, 1991.

Nakajima, T. Y., Suzuki, K., and Stephens, G. L.: Droplet growth in warm water clouds observed by the A-Train. Part I: Sensitivity analysis of the MODIS-derived cloud droplet sizes, J. Atmos. Sci., 67(6), 1884-1896, https://doi.org/10.1175/2009JAS3280.1, 2010.

NASEM: Thriving on Our Changing Planet: A Decadal Strategy for Earth *Observation from Space*, The National Academies Press, Washington, DC, 716pp, https://doi.org/10.17226/24938, 2018.

Norgren, M. S., Wood, J., Schmidt, K. S., van Diedenhoven, B., Stamnes, S. A., Ziemba, L. D., Crosbie, E. C., Shook, M. A., Kittelman, A. S., LeBlanc, S. E., Broccardo, S., Freitag, S., and Reid, J. S.: Above-aircraft cirrus cloud and aerosol optical depth from hyperspectral irradiances measured by a total-diffuse radiometer, Atmos. Meas. Tech., 15, 1373–1394, https://doi.org/10.5194/amt-15-1373-2022, 2022.

O'Connor, D., B. Baker, and R. P. Lawson, Upgrades to the FSSP-100 electronics. *Int. Conf. on Clouds and Precipitation*, Cancun, Mexico, IAMAS, http://cabernet.atmosfcu.unam.mx/ICCP-2008/abstracts/Program_on_line/Poster_13/O-Connor_extended.pdf, 2008.

Ohring, G., Wielicki, B., Spencer, R., Emery, B., and Datla, R.: Satellite instrument calibration for measuring global climate change: Report of a workshop, Bull. Amer. Meteor., 86, 1303–1314. https://doi.org/10.1175/bams-86-9-1303, 2005.

Painemal, D., and Zuidema, P.: Assessment of MODIS cloud effective radius and optical thickness retrievals over the Southeast Pacific with VOCALS-REx in situ measurements. J. Geophys. Res., 116, D24206, https://doi.org/10.1029/2011JD016155, 2011.

1125   Painemal, D., Spangenberg, D., Smith Jr., W. L., Minnis, P., Cairns, B., Moore, R. H., Crosbie, E., Robinson, C., Thornhill, K. L., Winstead, E. L., and Ziemba, L.: Evaluation of satellite retrievals of liquid clouds from the GOES-13 imager and MODIS over the midlatitude North Atlantic during the NAAMES campaign, Atmos. Meas. Tech., 14, 6633–6646, https://doi.org/10.5194/amt-14-6633-2021, 2021.

Platnick, S.: Vertical photon transport in cloud remote sensing problems, J. Geophys. Res., 105, 22919– 22935,
1130   https://doi.org/10.1029/2000JD900333, 2000.

Platnick, S., King, M., Ackerman, S., Menzel, W., Baum, B., Riedi, J., Frey, R.: The MODIS cloud products: Algorithms and examples from terra, IEEE Trans. Geosci. Remote Sens., 41, 459–473, https://doi.org/10.1109/tgrs.2002.808301, 2003.

Platnick, S., Meyer, K., Amarasinghe, N., Wind, G., Hubanks, P.A., Holz, R.E.: Sensitivity of Multispectral Imager
1135   Liquid Water Cloud Microphysical Retrievals to the Index of Refraction. Remote Sens., 12, 4165. https://doi.org/10.3390/rs12244165, 2020.

Platnick, S., Meyer, K., King, M. D., Wind, G., Amarasinghe, N., Marchant, B., Arnold, G. T., Zhang, Z., Hubanks, P. A., Holz, R. E., Yang, P., Ridgway, W. L., Riedi, J.: The MODIS Cloud Optical and Microphysical Products: Collection 6 Updates and Examples From Terra and Aqua, IEEE Trans. Geosci. Remote Sens., 55, 1, 502-525,
1140   https://doi.org/10.1109/TGRS.2016.2610522, 2017.

Platnick, S., Pincus, R., Wind, B., King, M. D., Gray, M. A., Hubanks, P. A.: An initial analysis of the pixel-level uncertainties in global MODIS cloud optical thickness and effective particle-size retrievals, Proc. SPIE 5652, Passive Optical Remote Sensing of the Atmosphere and Clouds IV, https://doi.org/10.1117/12.578353, 2004.

Platnick, S., and Valero, F. P. J.: A validation of a satellite cloud retrieval during ASTEX. J. Atmos. Sci., 52 (16),
1145   2985-3001 https://doi.org/10.1175/1520-0469(1995)0522.0.co;2, 1995.

Pinsky, M., and Khain, A.: Analytical investigation of the role of lateral mixing in the evolution of nonprecipitating cumulus. Part I: Developing clouds, J. Atmos. Sci., 77(3), 891-909, https://doi.org/10.1175/JAS-D-19-0036.1, 2020.

Rauber, R. M., Stevens, B., Ochs, H. T., III, Knight, C., Albrecht, B. A., Blyth, A. M., Fairall, C. W., Jensen, J. B.,
1150   Lasher-Trapp, S. G., Mayol-Bracero, O. L., Vali, G., Anderson, J. R., Baker, B. A., Bandy, A. R., Burnet, E., Brenguier, J.-L., Brewer, W. A., Brown, P. R. A., Chuang, R., Cotton, W. R., Di Girolamo, L., Geerts, B., Gerber, H., Göke, S., Gomes, L., Heikes, B. G., Hudson, J. G., Kollias, P., Lawson, R. R., Krueger, S. K., Lenschow, D. H., Nuijens, L., O'Sullivan, D. W., Rilling, R. A., Rogers, D. C., Siebesma, A. P., Snodgrass, E., Stith, J. L., Thornton, D. C., Tucker, S., Twohy, C. H., and Zuidema, P.: Rain in shallow cumulus over the ocean: The RICO
1155   campaign, Bull. Amer. Meteor. Soc., 88(12), 1912-1928, https://doi.org/10.1175/BAMS-88-12-1912, 1997.

Redemann, J., Wood, R., Zuidema, P., Doherty, S. J., Luna, B., LeBlanc, S. E., Diamond, M. S., Shinozuka, Y., Chang, I. Y., Ueyama, R., Pfister, L., Ryoo, J.-M., Dobracki, A. N., da Silva, A. M., Longo, K. M., Kacenelenbogen, M. S., Flynn, C. J., Pistone, K., Knox, N. M., Piketh, S. J., Haywood, J. M., Formenti, P., Mallet, M., Stier, P.,

1160 Ackerman, A. S., Bauer, S. E., Fridlind, A. M., Carmichael, G. R., Saide, P. E., Ferrada, G. A., Howell, S. G., Freitag, S., Cairns, B., Holben, B. N., Knobelspiesse, K. D., Tanelli, S., L'Ecuyer, T. S., Dzambo, A. M., Sy, O. O., McFarquhar, G. M., Poellot, M. R., Gupta, S., O'Brien, J. R., Nenes, A., Kacarab, M., Wong, J. P. S., Small-Griswold, J. D., Thornhill, K. L., Noone, D., Podolske, J. R., Schmidt, K. S., Pilewskie, P., Chen, H., Cochrane, S. P., Sedlacek, A. J., Lang, T. J., Stith, E., Segal-Rozenhaimer, M., Ferrare, R. A., Burton, S. P., Hostetler, C. A., Diner, D. J., Seidel, F. C., Platnick, S. E., Myers, J. S., Meyer, K. G., Spangenberg, D. A., Maring, H., and

1165 Gao, L.: An overview of the ORACLES (ObseRvations of Aerosols above CLouds and their intEractionS) project: aerosol–cloud–radiation interactions in the southeast Atlantic basin, Atmos. Chem. Phys., 21, 1507–1563, https://doi.org/10.5194/acp-21-1507-2021, 2021.

Romps, D. M., and Vogelmann, A. M.: Methods for estimating 2D cloud size distributions from 1D observations, J. Atmos. Sci., 74(10), 3405-3417, https://doi.org/10.1175/JAS-D-17-0105.1, 2017.

1170 Ross, A.D., Holz, R.E., Quinn, G., Reid, J. S., Xian, P., Turk, F. J., and Posselt, D. J.: Exploring the first aerosol indirect effect over Southeast Asia using a 10-year collocated MODIS, CALIPSO, and model dataset, Atmos. Chem. Phys., 18, 12747-12764. https://doi.org/10.5194/acp-18-12747-2018, 2018.

Rossow, W. B., and Schiffer, R. A.: ISCCP cloud data products, Bull. Amer. Meteor. Soc., 72(1), 2–20. https://doi.org/10.1175/1520-0477(1991)072<0002:ICDP>2.0.CO;2, 1991.

1175 Sauvageot, H., and Omar, J.: Radar reflectivity of cumulus clouds, J. Atmos. Ocean. Technol., 4(2), 264-272, https://doi.org/10.1175/1520-0426(1987)004<0264:RROCC>2.0.CO;2, 1987.

Shang, H., Chen, L., Bréon, F. M., Letu, H., Li, S., Wang, Z., and Su, L.: Impact of cloud horizontal inhomogeneity and directional sampling on the retrieval of cloud droplet size by the POLDER instrument, Atmos. Meas. Tech., 8, 4931–4945, https://doi.org/10.5194/amt-8-4931-2015, 2015.

1180 Sinclair, K., van Diedenhoven, B., Cairns, B., Yorks, J., Wasilewski, A., and McGill, M.: Remote sensing of multiple cloud layer heights using multi-angular measurements, Atmos. Meas. Tech., 10, 2361–2375, https://doi.org/10.5194/amt-10-2361-2017, 2017.

Suzuki, K., Golaz, J. -C., and Stephens, G. L.: Evaluating cloud tuning in a climate model with satellite observations, Geophys. Res. Lett., 40, 4464–4468, https://doi.org/10.1002/grl.50874, 2013.

1185 Tan, I., Oreopoulos, L. and Cho, N.: The role of thermodynamic phase shifts in cloud optical depth variations with temperature. Geophys. Res. Lett., 46, 4502–4511, https://doi.org/10.1029/2018GL081590, 2019.

Tanelli, S., Durden, S. L., Im, E., Pak, K. S., Reinke, D. G., Partain, P., Haynes, J. M., and Marchand, R. T.: CloudSat's cloud profiling radar after two years in orbit: Performance, calibration, and processing, IEEE Trans. Geosci. Remote Sens., 46, 11, 3560-3573, https://doi.org/10.1109/TGRS.2008.2002030, 2008.

1190 van Diedenhoven, B., Fridlind, A. M., Ackerman, A. S., and Cairns, B.: Evaluation of hydrometeor phase and ice properties in cloud-resolving model simulations of tropical deep convection using radiance and polarization measurements, J. Atmos. Sci., 69(11), 3290-3314, https://doi.org/10.1175/JAS-D-11-0314.1, 2012.

Vant-Hull, B., Marshak, A., Remer, L. A., and Li, Z.: The effects of scattering angle and cumulus cloud geometry on satellite retrievals of cloud drop effective radius. IEEE Trans. Geosci. Remote Sens., 1039–1045.

1195 https://doi.org/10.1109/TGRS.2006.890416, 2007.

Várnai, T., and Davies, R.: Effects of cloud heterogeneities on shortwave radiation: Comparison of cloud-top variability and internal heterogeneity. J. Atmos. Sci., 56, 4206–4224, https://doi.org/10.1175/1520-0469(1999)056<4206:EOCHOS>2.0.CO;2, 1999.

Wang J.Y. and Geerts, B.: Identifying drizzle within marine stratus with W-band radar reflectivity profiles. Atmos. Res., 69, 1-27, https://doi.org/10.1016/j.atmosres.2003.08.001, 2003.

Werner, F., Zhang, Z., Wind, G., Miller, D. J., and Platnick, S.: Quantifying the impacts of subpixel reflectance variability on cloud optical thickness and effective radius retrievals based on high-resolution ASTER observations. J. Geophys. Res. Atmos., 123, 4239–4258, https://doi.org/10.1002/2017JD027916, 2018a.

Werner, F., Zhang, Z., Wind, G., Miller, D. J., Platnick, S., and Di Girolamo, L.: Improving cloud optical property retrievals for partly cloudy pixels using coincident higher–resolution single band measurements: A feasibility study using ASTER observations, J. Geophys. Res., 123, 12253—12276, https://doi.org/10.1029/2018JD028902, 2018b.

Witte, M. K., Yuan, T., Chuang, P. Y., Platnick, S., Meyer, K. G., Wind, G., and Jonsson, H. H.: MODIS retrievals of cloud effective radius in marine stratocumulus exhibit no significant bias. Geophys. Res. Lett., 45, 10,656–10,664. https://doi.org/10.1029/2018GL079325, 2018.

Zhang, S., Xue, H., and Feingold, G.: Vertical profiles of droplet effective radius in shallow convective clouds, Atmos. Chem. Phys., 11, 4633–4644, https://doi.org/10.5194/acp-11-4633-2011, 2011.

Zhang, Z., Ackerman, A. S., Feingold, G., Platnick, S., Pincus, R., and Xue, H.: Effects of cloud horizontal inhomogeneity and drizzle on remote sensing of cloud droplet effective radius: Case studies based on large-eddy simulations, J. Geophys. Res., 117, D19208, https://doi.org/10.1029/2012JD017655, 2012.

Zhang, Z., and Platnick, S.: An assessment of differences between cloud effective particle radius retrievals for marine water clouds from three MODIS spectral bands, J. Geophys. Res., 116, D20215, https://doi.org/10.1029/2011JD016216, 2011.

Zhang, Z., Werner, F., Cho, H. M., Wind, G., Platnick, S., Ackerman, A. S., Di Girolamo, L., Marshak, A., and Meyer K.: A framework based on 2-D Taylor expansion for quantifying the impacts of sub-pixel reflectance variance and covariance on cloud optical thickness and effective radius retrievals based on the bi-spectral method, J. Geophys. Res. -Atmos., 121, https://doi.org/10.1002/2016JD024837, 2016.

Zhao, G., and Di Girolamo, L.: Statistics on the macrophysical properties of trade wind cumuli over the tropical western Atlantic, J. Geophys. Res., 112, D10204, https://doi.org/10.1029/2006JD007371, 2007.

Zhuge, X., Zou, X. and Wang, Y.: AHI-Derived Daytime Cloud Optical/Microphysical Properties and Their Evaluations With the Collection-6.1 MOD06 Product, IEEE Trans. Geosci. Remote Sens., 59, 8, 6431-6450, https://doi.org/10.1109/TGRS.2020.3027017, 2021.

Zinner, T., Wind, G., Platnick, S., and Ackerman, A. S.: Testing remote sensing on artificial observations: impact of drizzle and 3-D cloud structure on effective radius retrievals, Atmos. Chem. Phys., 10, 9535–9549, https://doi.org/10.5194/acp-10-9535-2010, 2010.